AD-A158 080 PERFORMANCE AND PREDICTIONS FOR A LARGE BLAST SIMULATOR 1/1
MODEL(U) ARMY BALLISTIC RESEARCH LAB ABERDEEN PROVING
GROUND MD D M HISLEY ET AL. APR 85 BRL-TR-2647

UNCLASSIFIED F/G 14/2 NL

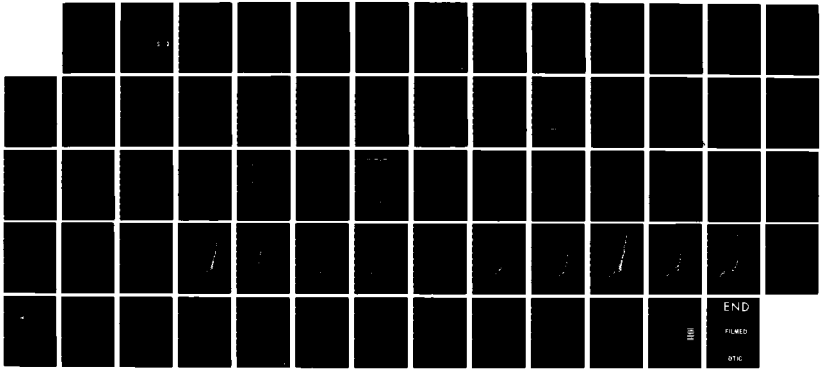

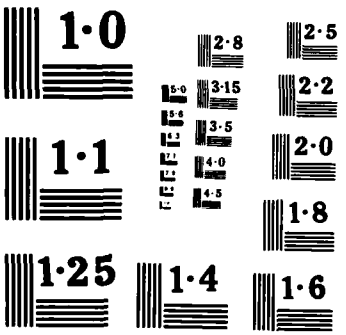

(2)

AD

US ARMY MATERIEL COMMAND

TECHNICAL REPORT BRL-TR-2647

PERFORMANCE AND PREDICTIONS FOR A LARGE BLAST SIMULATOR MODEL

Dixie M. Hisley
Edmund J. Gion
Brian P. Bertrand

April 1985

US ARMY BALLISTIC RESEARCH LABORATORY
ABERDEEN PROVING GROUND, MARYLAND

JW

Destroy this report when it is no longer needed.
Do not return it to the originator.

Additional copies of this report may be obtained from the National Technical Information Service, U. S. Department of Commerce, Springfield, Virginia 22161.

The findings in this report are not to be construed as an official Department of the Army position, unless so designated by other authorized documents.

The use of trade names or manufacturers' names in this report does not constitute indorsement of any commercial product.

UNCLASSIFIED

SECURITY CLASSIFICATION OF THIS PAGE *(When Data Entered)*

REPORT DOCUMENTATION PAGE		READ INSTRUCTIONS BEFORE COMPLETING FORM
1. REPORT NUMBER Technical Report BRL-TR-2647	2. GOVT ACCESSION NO. AD-A158080	3. RECIPIENT'S CATALOG NUMBER
4. TITLE *(and Subtitle)* PERFORMANCE AND PREDICTIONS FOR A LARGE BLAST SIMULATOR MODEL		5. TYPE OF REPORT & PERIOD COVERED Final 6. PERFORMING ORG. REPORT NUMBER
7. AUTHOR*(s)* Dixie Hisley Edmund Gion Brian Bertrand		8. CONTRACT OR GRANT NUMBER*(s)*
9. PERFORMING ORGANIZATION NAME AND ADDRESS US Army Ballistic Research Laboratory ATTN: AMXBR-TBD Aberdeen Proving Ground, MD 21005-5066		10. PROGRAM ELEMENT, PROJECT, TASK AREA & WORK UNIT NUMBERS Project # 1L162120AH25 1L162618AH80
11. CONTROLLING OFFICE NAME AND ADDRESS US Army Ballistic Research Laboratory ATTN: AMXBR-OD-ST Aberdeen Proving Ground, MD 21005-5066		12. REPORT DATE April 1985 13. NUMBER OF PAGES 64
14. MONITORING AGENCY NAME & ADDRESS*(if different from Controlling Office)*		15. SECURITY CLASS. *(of this report)* UNCLASSIFIED 15a. DECLASSIFICATION/DOWNGRADING SCHEDULE

16. DISTRIBUTION STATEMENT *(of this Report)*

Approved for public release; distribution unlimited.

17. DISTRIBUTION STATEMENT *(of the abstract entered in Block 20, if different from Report)*

18. SUPPLEMENTARY NOTES

19. KEY WORDS *(Continue on reverse side if necessary and identify by block number)*

Blast Waves
Blast Simulation
NASA-ames Code
Large Blast Simulators
Shock Tubes
Shock Pressures

20. ABSTRACT *(Continue on reverse side if necessary and identify by block number)*

An attempt is made ~~herein~~ to verify the predictions from a 1-D BRL Code against the flow from a complicated, non-straight shock tube configuration; the code then could be utilized for future Large Blast/Thermal Simulator (LB/TS) design and prediction of performance. The shock tube is a 1/37 scale, axisymmetric model following the design for a multi-driver large blast simulator (LBS) located at Centre d'Etude, Gramat, France. It is used to produce shock pressures from 3.1 to 31 psi (21 to 214 kPa) and characteristic decaying wave forms. The

DD FORM 1 JAN 73 1473 EDITION OF 1 NOV 65 IS OBSOLETE

UNCLASSIFIED

SECURITY CLASSIFICATION OF THIS PAGE *(When Data Entered)*

BRL code is a quasi-one-dimensional, adiabatic, inviscid, Eulerian computer algorithm. The code is described and some preliminary checks against related configurations are performed. Furthermore, the code uses the experimental tube geometry and run conditions to generate flow data for comparison with the experimental data.

Additionally, parameter studies are done--necking down of nozzle throat at the diaphragm station, heating of the driver gas, temperature effect on driver due to pressurizing--to check their influence on the tube behavior.

In general, computed wave forms as well as levels agree well with experiment except for the highest levels where head losses and real gas effects are more pronounced. With the natural-burst-of-diaphragm operation of tube, diaphragm blockage of the nozzle throat is a problem; temperature effects due to pressurizing of driver are not.

TABLE OF CONTENTS

LIST OF ILLUSTRATIONS

LIST OF ILLUSTRATIONS (Continued)

I. INTRODUCTION

This report deals with calculations and measurements performed to verify a conceptual 1-D computational model of a multi-driver, "non-straight" shock tube. The interest lies in the Army's perceived need for a large blast thermal simulator (LB/TS), (a) to reduce dependence on large scale, expensive HE nuclear simulations, with attendant supply, weather, and coordination problems, and limitation to low yields, and (b) to have available a facility capable of testing through the entire tactical nuclear threat range. To guide U.S. development and to assure meeting U.S. requirements in a cost-effective manner, computations and small scale experiments are necessary to assess design and performance of possible LB/TS configurations.

Currently there exists a number of smaller blast- and shock-tubes located the U.S., Britain, Germany, and France. In particular, an operational rge blast simulator (LBS) facility located at Centre d' Etude, Gramat (CEG), France,[1,2] incorporates a number of advanced design concepts and is of a unique multi-driver design. The theoretical modelling of this facility has been reported earlier.[3]

We note the interesting calculations and experiments by H.O. Amann,[4,5] who also treats a multi-driver configuration for a large shock tube: nozzles are attached to high pressure bottles of equal length. In his calculations Amann lumps the nozzle openings into a single opening and treats the gas flow one-dimensionally. This model configuration is different from that described here and the decaying blast wave simulation is not considered.

In the following sections we will describe first the experimental efforts and results, then the computational effort and its results. A comparison will then be made of the experimental/computational results.

---

[1] *J.R. Crosner and J.B.G. Monzac, "Large Diameter High Performance Blast Simulators." Proc. Fifth Int'l Symposium on Military Applications of Blast Simulation, Vol. 1, Stockholm, Sweden, May 23-26, 1977.*

[2] *S. Gratias and J.B.G. Monzac, "The Large-Scale Nuclear Blast Simulator of the Gramat Research Center-Concept, Research, Performance." Proc.Seventh Int'l. Symposium on Military Applications of Blast Simulation, Medicine Hat, Canada, July 13-17, 1981.*

[3] *A.Mark, "Computational Design of Large Scale Blast Simulators." AIAA 19th Aerospace Sciences Meeting. St. Louis, Missouri, January 12-15, 1981.*

[4] *H.O.Amann, "Theoretical and Experimental Investigations on the Driving Mechanism of a Shock Wave Simulator of Large Cross Section." Ernest Mach Institute Freiburg, W. Germany, Report No. 2/72 May 1972.*

[5] *H.O.Amann, "Model Tests for a Large Diameter Simulator Driven by Several Generators Filled with Compressed Air." Proc. Fifth Int'l. Symposium on Military Applications of Blast Simulation, Vol. 1, Stockholm, May 23-26, 1977.*

II. EXPERIMENTAL SHOCK TUBE AND PROCEDURES

A. LBS Model and Instrumentation

The multi-driver CEG facility, as depicted in Figure 1a, is modeled by the 2-dimensional, axi-symmetric shock tube shown schematically in Figure 1b. The circular cross-section of the driver in Figure 1b at any axial location is the total cross-sectional area of the multi-driver configuration at the corresponding location. The stepped driver then results. The 2-dimensional axisymetric LBS shocktube was constructed to 1/37 scale, and is the physical representation for the computational model.

A conical nozzle of 16^{o} half angle represents the lumping of the seven 6^{o} half angle nozzles of the CEG configuration. Three piezoelectric transducers in the nozzle wall, spaced at one inch (2.54 cm) intervals from the nozzle opening, monitor pressure development in the nozzle. The nozzle opens into a 10 inch (25.4 cm) diameter driven tube which may be closed off to the atmosphere by a removable annular plate fastened to the nozzle opening. This feature permitted duplicating the CEG facility's removal of their similar closure plate for those shock overpresures where the rearward-facing shock was expected to be swept downstream and out of the nozzle.[2] Removal of the annulus plate for these levels allows air to be entrained into the flow following the shock, thereby extending the positive duration.

The test section/driven tube was instrumented along the wall with piezoelectric gages at one diameter intervals beginning at one diameter downstream of the nozzle opening. Station numbers thus correspond to distance in diameters down the driven tube. Additionally, a pitot probe (also a piezoelectric gage) was installed at Station 7S, in radially 1/4 diameter and seven diameters downstream of the nozzle and across from Station 7, the test section location corresponding to that of the CEG facility. The driven tube was a standard10 inch (25 cm), Schedule 40 seamless steel pipe, of 18 feet (5.5 m) stock length. The length was left intact to observe the lengthening of test time/wave duration before the end-rarefaction wave's arrival back at the test station.

The shock tube driver was pressurized through a regulator and manually operated solenoid valve. The driver pressure at diaphragm burst was monitored by a Bytrex-type gage through an orifice tube communicating through the breech plug to the driver volume. This gage was connected to a peak reading meter calibrated to read out the pressures directly. Various thicknesses of Mylar and aluminum diaphragms were used to obtain a range of driver pressures. The data from 13 pressure channels were taken to an analog tape recorder according to a basic data acquisition scheme, Figure 2, which also shows the scheme for data reduction.

The firing procedure called for pressurizing the diaphragm to its natural rupture point. Some questions about the "equilibrium" state of the driver gas were raised in view of noise and discrepancies between prediction and experiment. Subsequent tests using thermocouples in the driver to monitor typical temperatures during simulated runs will be presented. These will demonstrate the negligible temperature effects during pressurizing as well as an axial

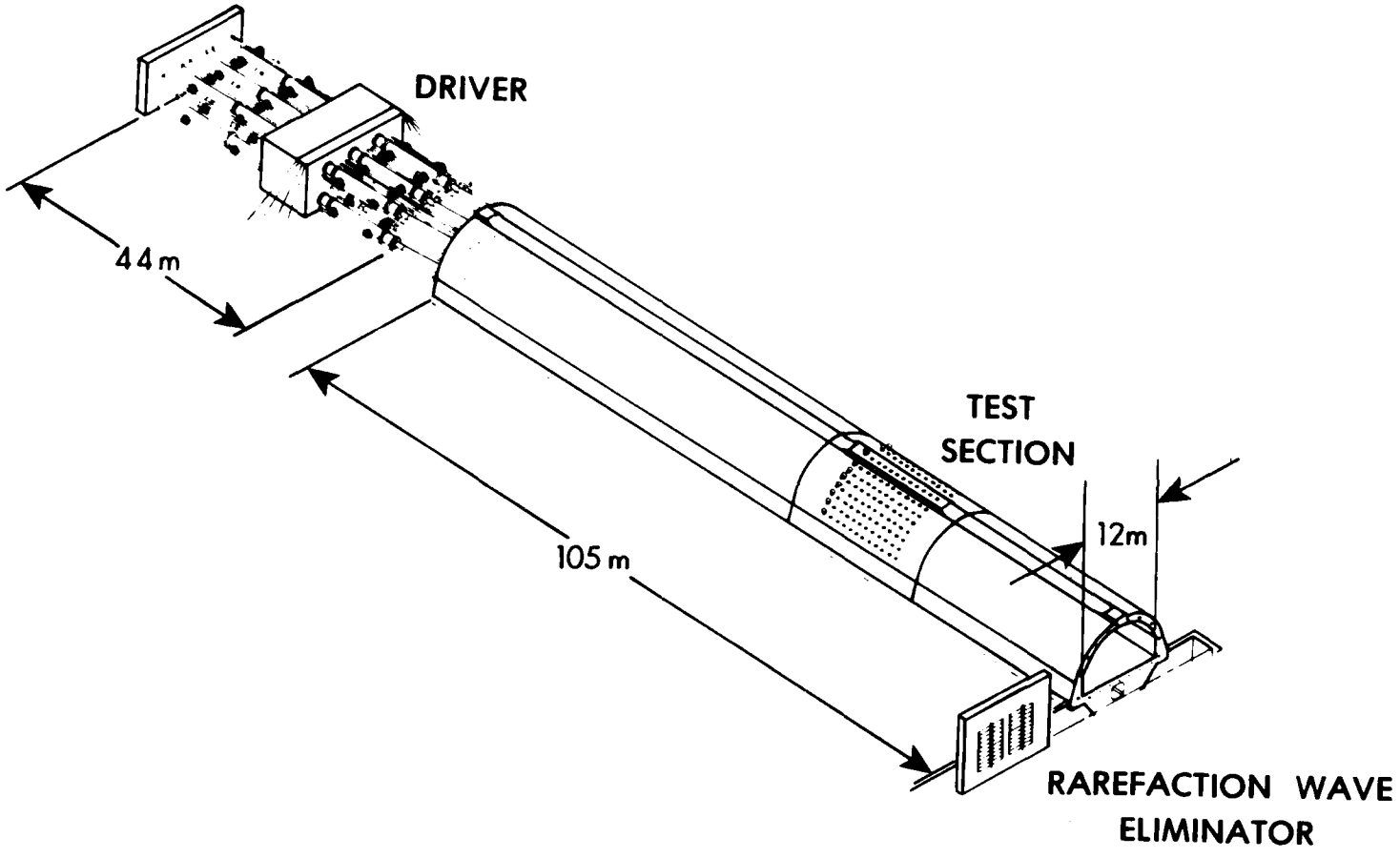

Figure 1. Shock Tube Configurations

a. Multi-Driver Shock Tube, CEG, France

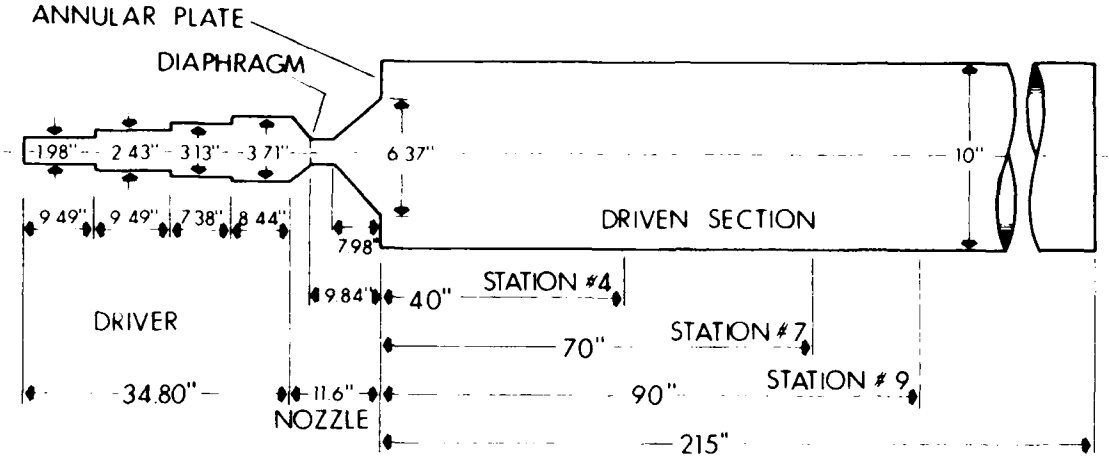

b. Axisymmetric Computational Model

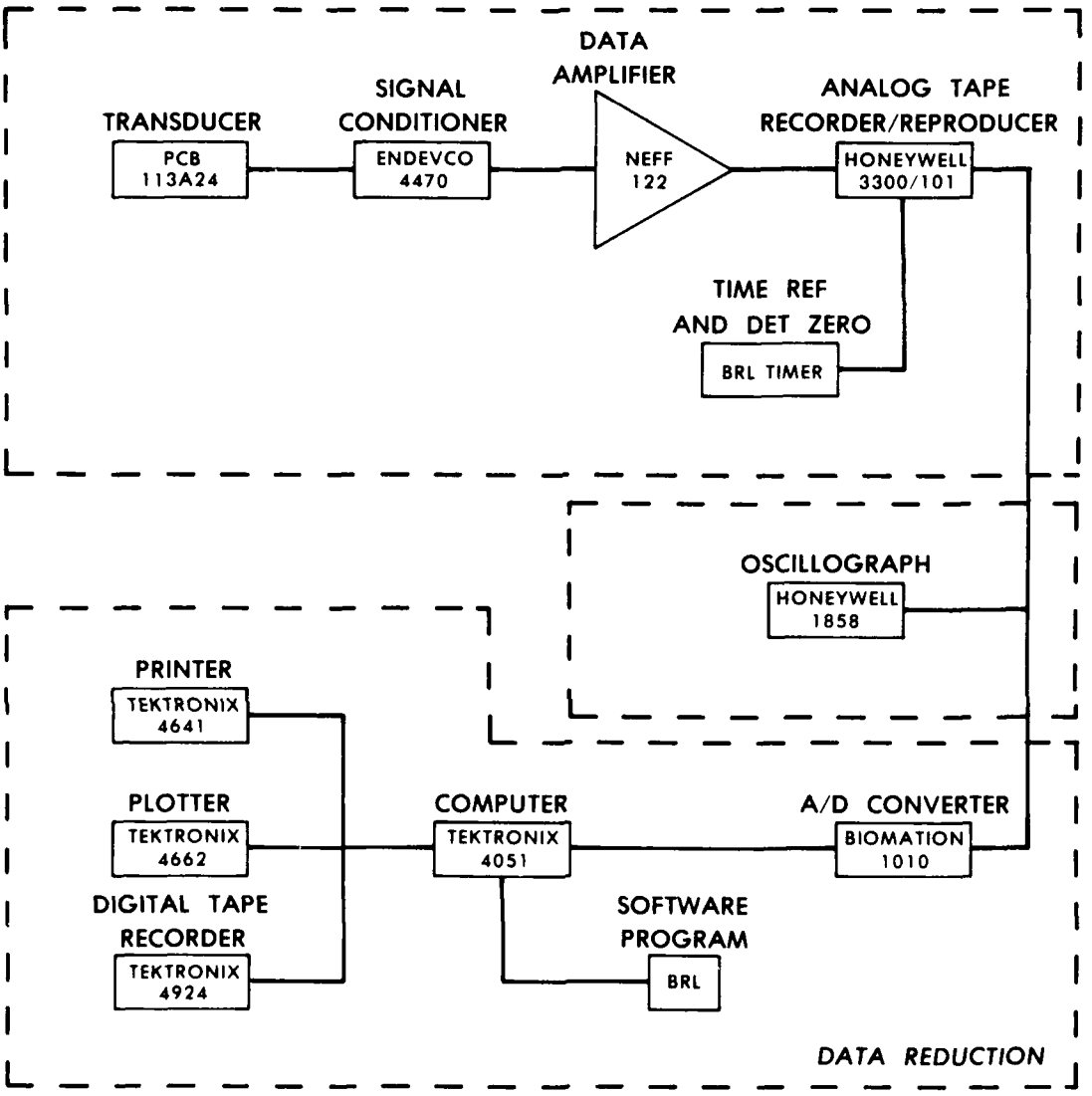

Figure 2. Data Acquisition Scheme

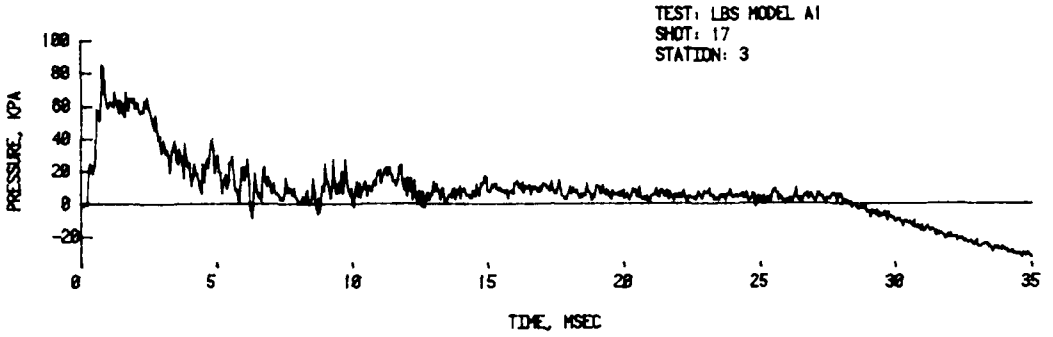

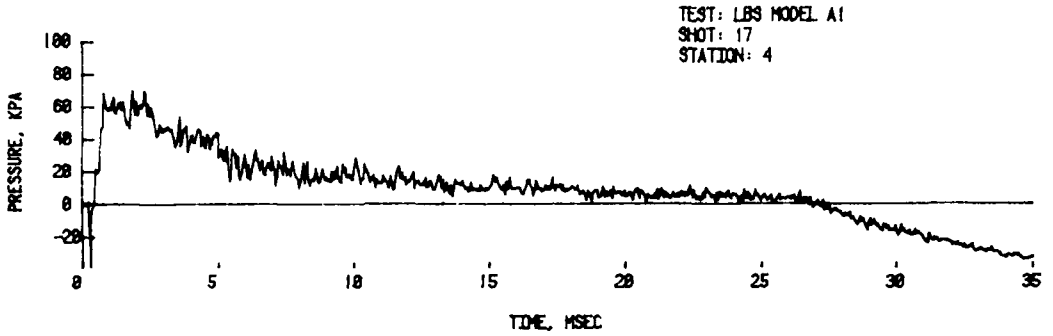

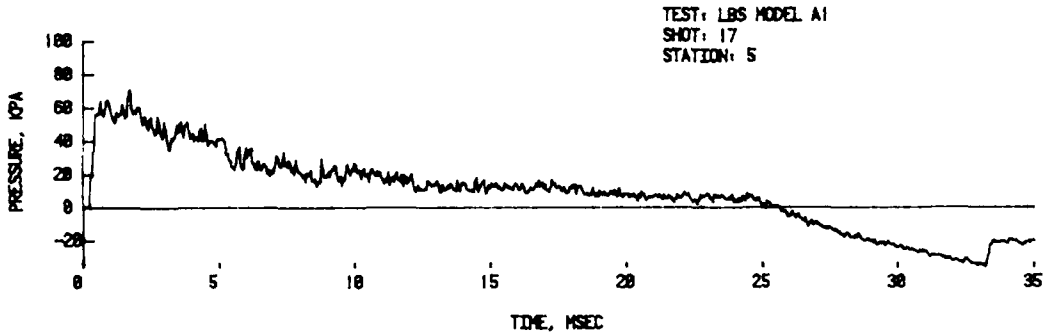

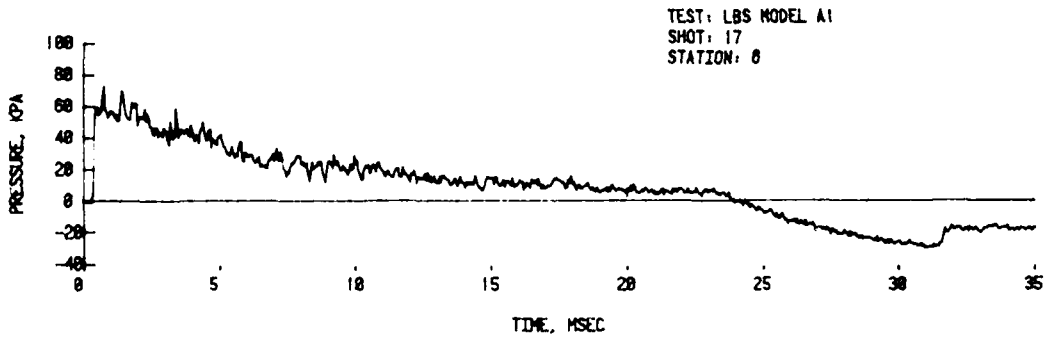

b. Low Level Shock Flow (cont.)

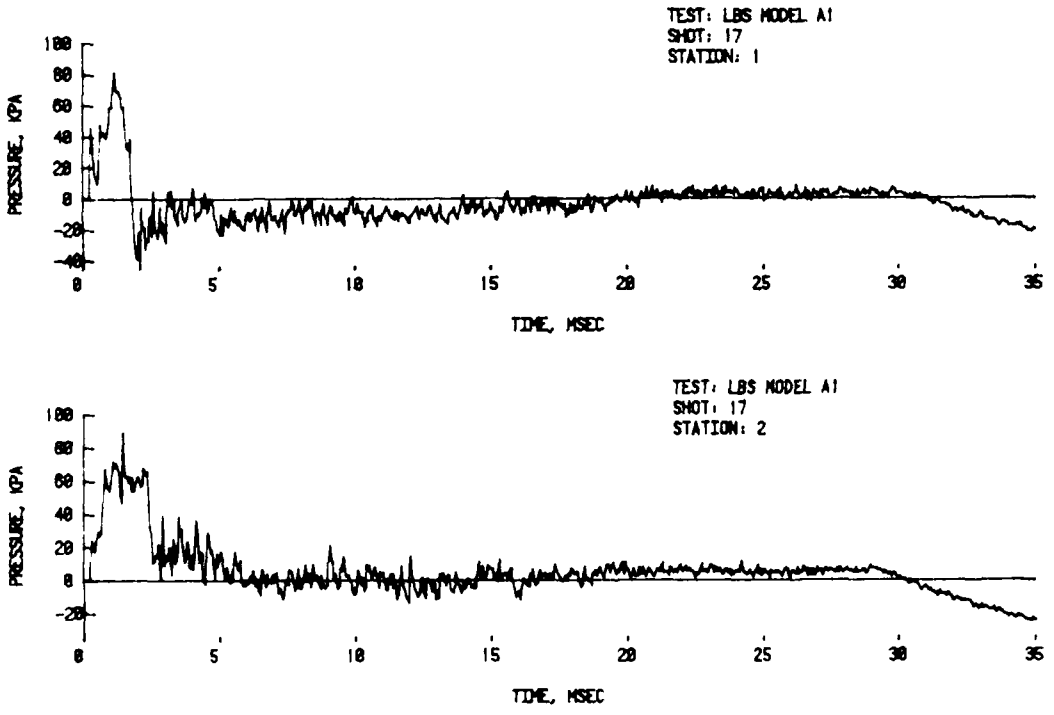

b. Low Level Shock Flow

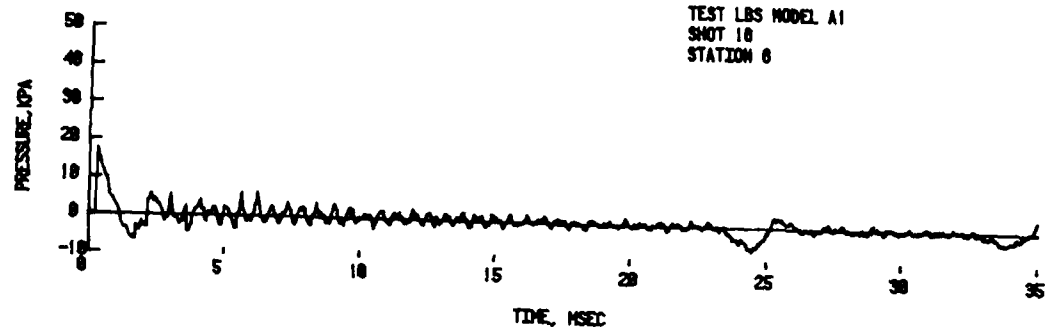

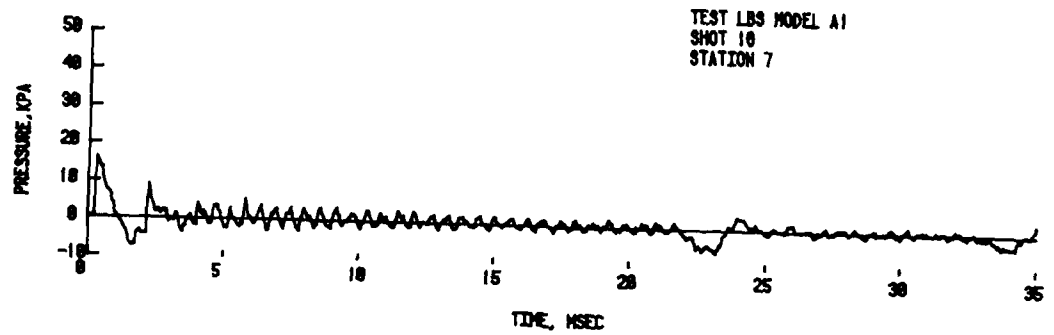

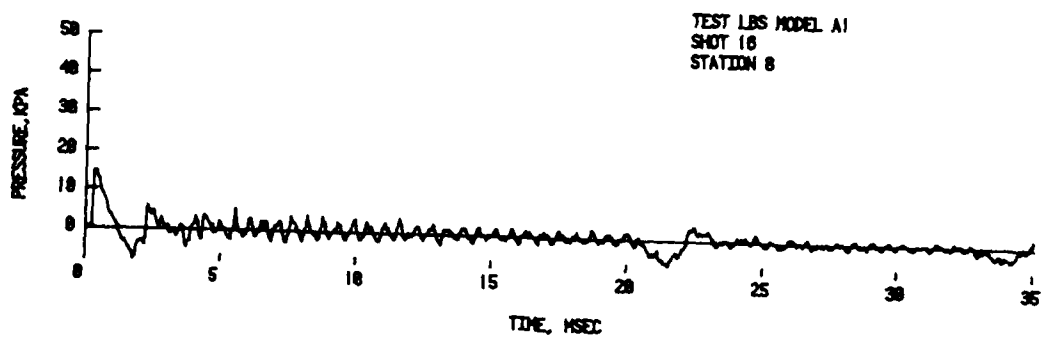

Figure 7. Shots With Detonator Burst of Diaphragm

a. No Flow

3. Detonator-Burst of Diaphragm. Additionally, tests were performed with breakage of the diaphragm by standard detonators (Reynolds Industries RP-87-Exploding Bridge Wire Detonators). The relevant Shots are 16-18, Figure 7. These were performed to determine the detonator's disturbance to the flow. They anticipate use of detonators to rupture the diaphragms in a future multi-driver shock tube model: respectively, 7a) detonator only, no flow; 7b) detonator with a low level shock pressure, where detonator effects would be most noticeable; and 7c) detonator with a high level shock pressure.

The result in the no-flow situation, Figure 7a, shows a detonation shock of small-impulse moving through the test section. For the weaker flow situation, Figure 7b, the detonation spike merges with the primary shock and has no separate identity beyond Station 5. Similarly, for the high level shock, Figure 7c, the detonation spike is detected only to Station 6. In both cases detonator perturbations appear no greater than the noise appearing on the traces.

Additionally, one may, in Figure 8a, compare this shot, at Test Station 7 (without annulus plate) with similar level, natural-burst diaphragm shots, without and with annulus plate, respectively, Figure 8b and c. The set of results indicate that use of a small detonator to rupture the diaphragm has negligible effect on test station pressure level and waveform.

4. Diaphragm Blockage of Nozzle Opening. In the shots at the highest driver pressures, it was noted that the recorded shock pressures were not increasing as expected. The suspicion was of "necking down" of the required thicker diaphragms by the downstream nozzle wall. As a check a few burst diaphragms were examined for effective open area relative to the (design) nozzle throat area. This was accomplished by imaging the open area in parallel light and measuring. The numbers appear in the Table 2, which suggests a substantial blockage with the thicker diaphragms.

TABLE 2. BURST DIAPHRAGM OPEN AREA

Shot	P_4/P_1	Matl	Thickness (mil)	% Open Area
3	29	Alum	20	89
12	136	Alum	84	70
14	137	Alum	84	67
15	179	Alum	104	63

The downstream nozzle throat section had originally been relieved to accomodate 20 mil diaphragms (1.900" vs 1.86"D). Subsequently, it was bored out to 2.20"D to permit use of our thickest diaphragms. The last shots 21-23 were made with this more open downstream throat. These runs resulted in the higher shock pressures with increasing driver pressures, as would be expected.

The next sections will describe the computer modeling efforts and will present comparisons between computations and experiment.

Text continued on page 31

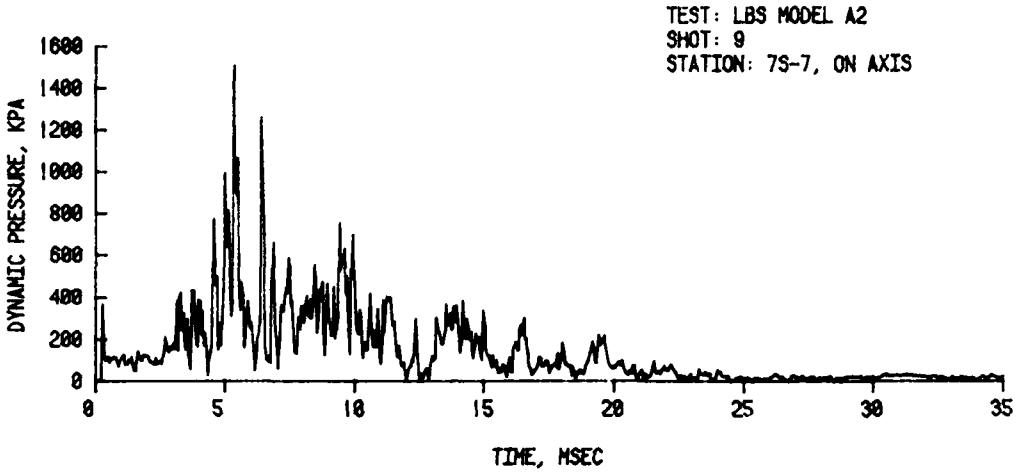

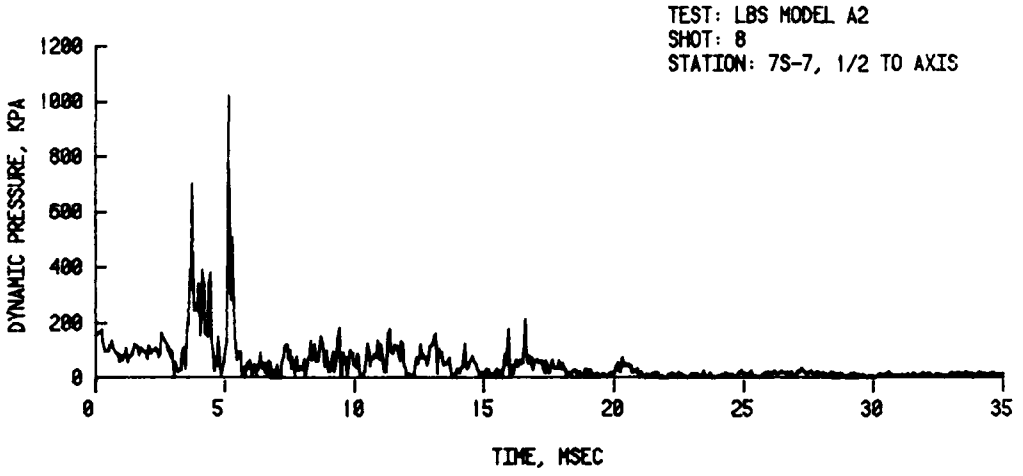

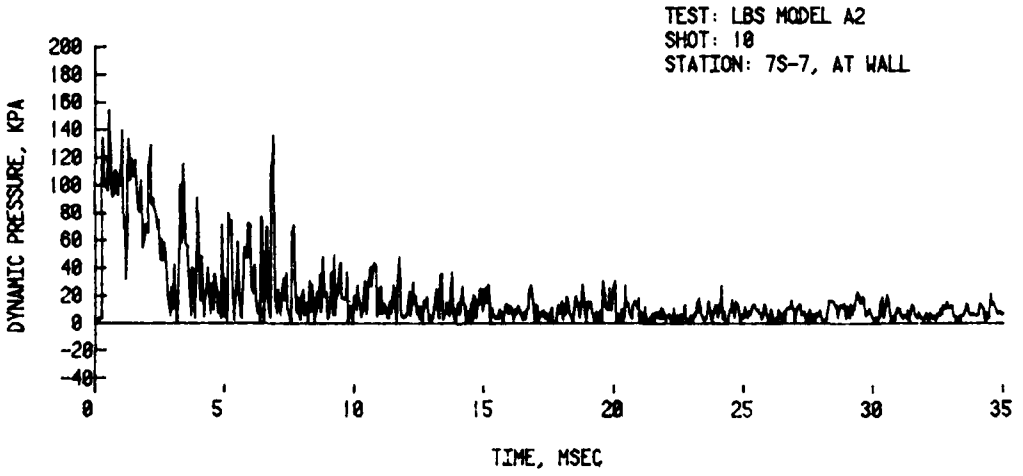

Figure 6. Dynamic Pressure at Different Pitot Probe Positions

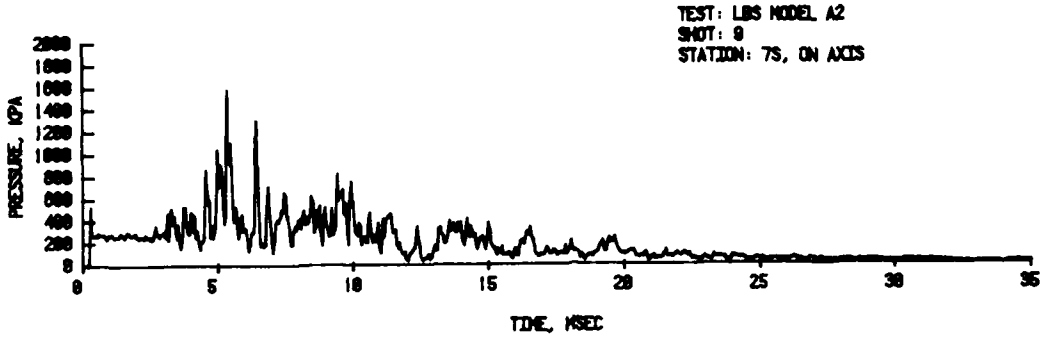

a. Probe on Axis, Annulus Plate Out

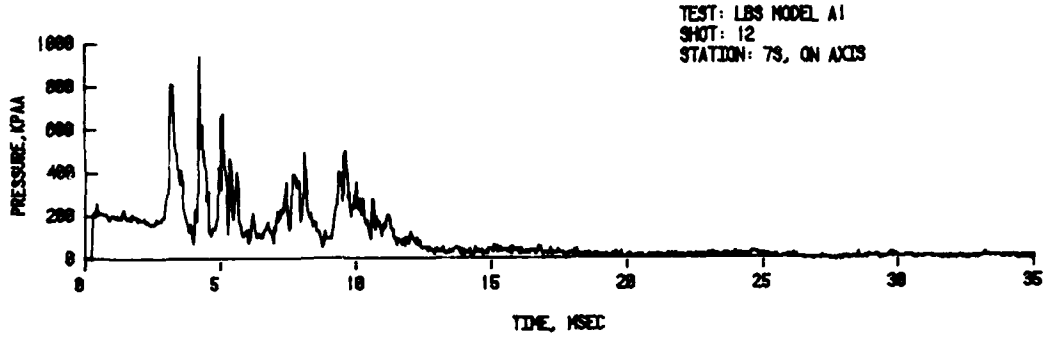

b. Probe on Axis, Annulus Plate In

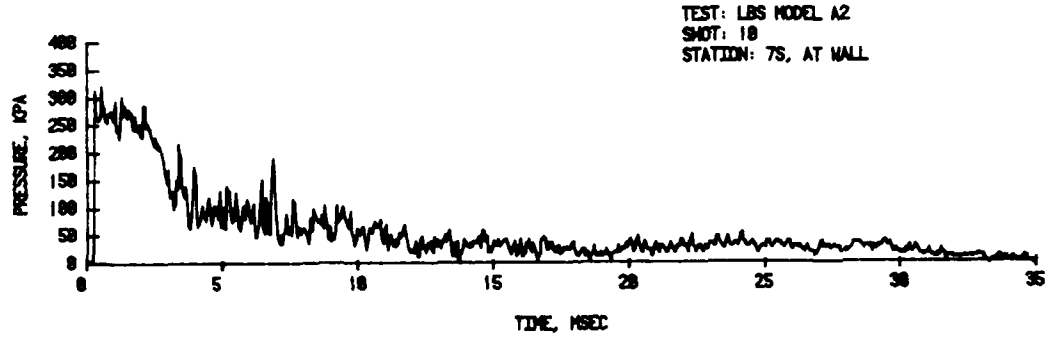

c. Probe Near Wall, Annulus Plate Out

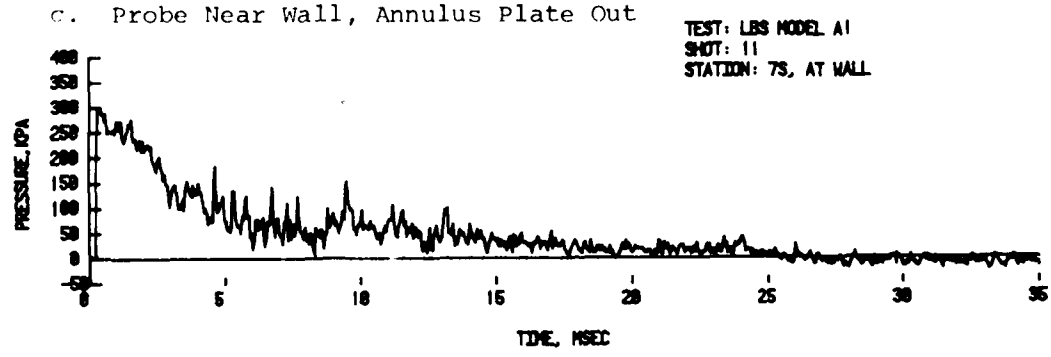

d. Probe Near Wall, Annulus Plate In

Figure 5. Comparison of Stagnation Pressures

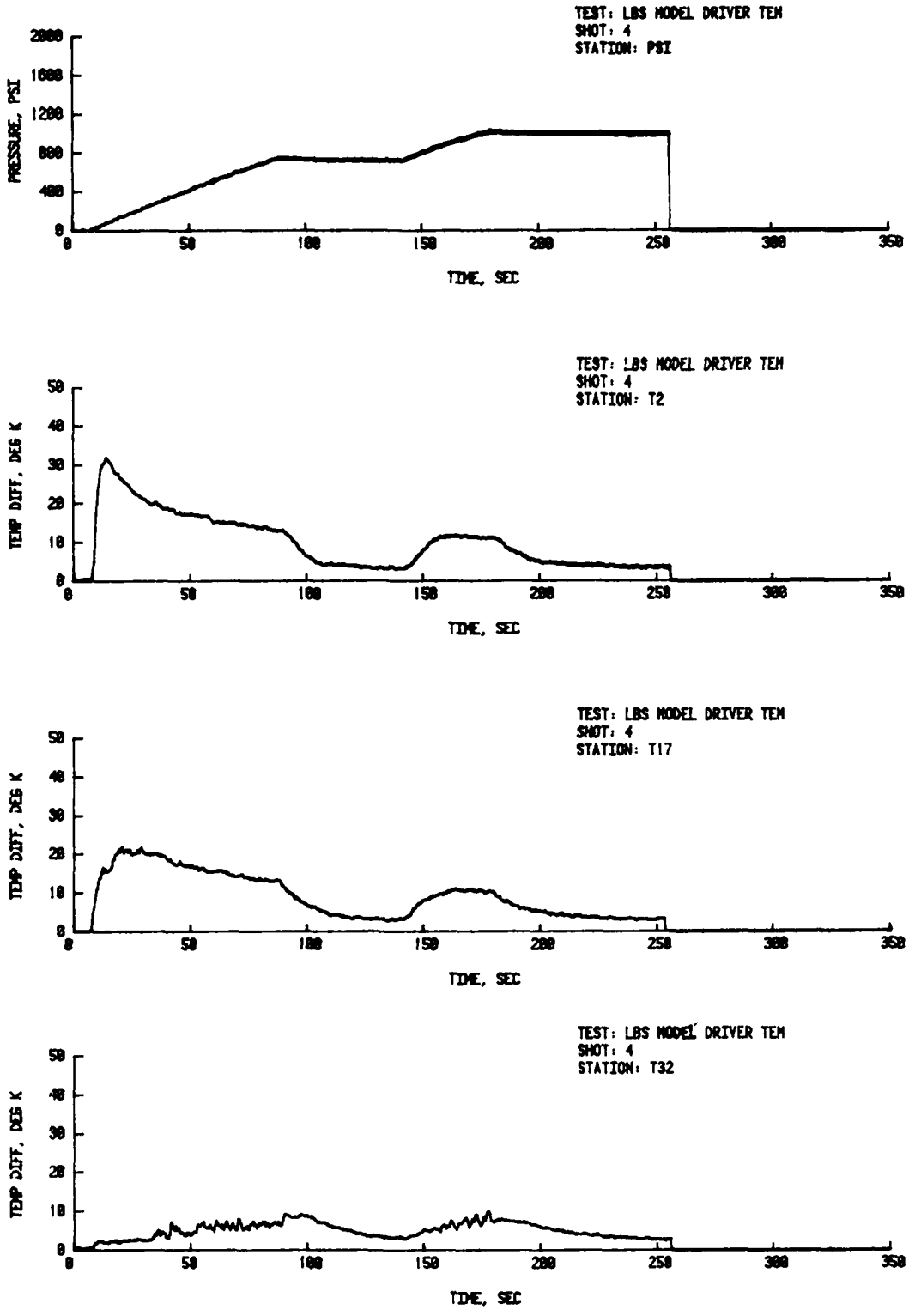

Figure 4. Driver Gas Temperature during Pressurizing

Results are shown for a mid-level pressure, Figure 4; other results are similar. The driver-pressure record shows one or more plateaus, allowing gas to equilibrate or simulating the pause allowing tape recorder to come to speed, then the final pressure rise to and beyond the natural burst pressure, here 65 atm. or 950 psi. The resulting temperatures at the three locations are exhibited. At the station T2 next to the diaphragm and farthest from the air inlet an initial sharp rise due to pressurization is terminated by cooling to the walls and mixing with already present gas, with more rapid cooling when pressurization is stopped (no fresh heat addition) for the tape recorder. A second rise follows when pressurization is resumed, to carry driver pressure to beyond the natural burst point, whereupon the experiment ceases.

The maximum driver temperature thus should be ~ 12 ^{o}K above ambient, for this mid-level shot. The gas temperatures nearer the air inlet stations, T17 and T32, are seen to be lower during the filling process. At the highest pressure run, the maximum temperature was 40 ^{o}K above ambient, while at dia phragm burst the temperature was again ~ 10-12 ^{o}K. Thus it is concluded that temperature effects were an insignificant factor in experimental/theoretical discrepancies.

2. Stagnation Pressures. It is of interest to examine the stagnation pressure records, Station 7s. The stagnation pressure offers a simple means to detect density differences in the flow not seen by the wall pressure gage. As was seen in Shot 7, Figure 3, and succeeding shots, the cold driver gas arrives at the test station before observation time terminates. (Heating of the driver gas to match interface conditions and/or to alleviate cold gas effects is looked at in the theoretical section; experimental results will be obtained and reported at a later date.)

Figure 5 shows results at similar run conditions for the stagnation probe located on axis when the annulus plate is out (LBS Model "A2")-(a), and when annulus plate is in (LBS Model "A1")-(b). The stagnation probe is moved next to the wall in (c) and (d), respectively, for a similar comparison. On axis, the stagnation probe sees a somewhat different, less noisy region of cold gas for the closed annulus plate "in"- configuration than for the "out" configuration. This result is reasonable since there is no entrained air to mix with the driver gas flow. The differences are less obvious with the stagnation probe next to the wall. It is clear that stagnation pressures recorded near the wall do not reflect the actual conditions a test target would be exposed to (were the air entrainment confined to the tube periphery as in our 1-D modelling). (The actual CEG facility's configuration, however, would permit a more uniform air entrainment over the cross section.)

A comparison of the dynamic pressures, labelled Station 7s - 7, Figure 6, derived from the stagnation probe positions on axis-(a), midway to axis(the normal position)-(b), and next to wall-(c), illustrates the significant variation in loadings with cold driver gas arrival at the test station.

Text continued page 22

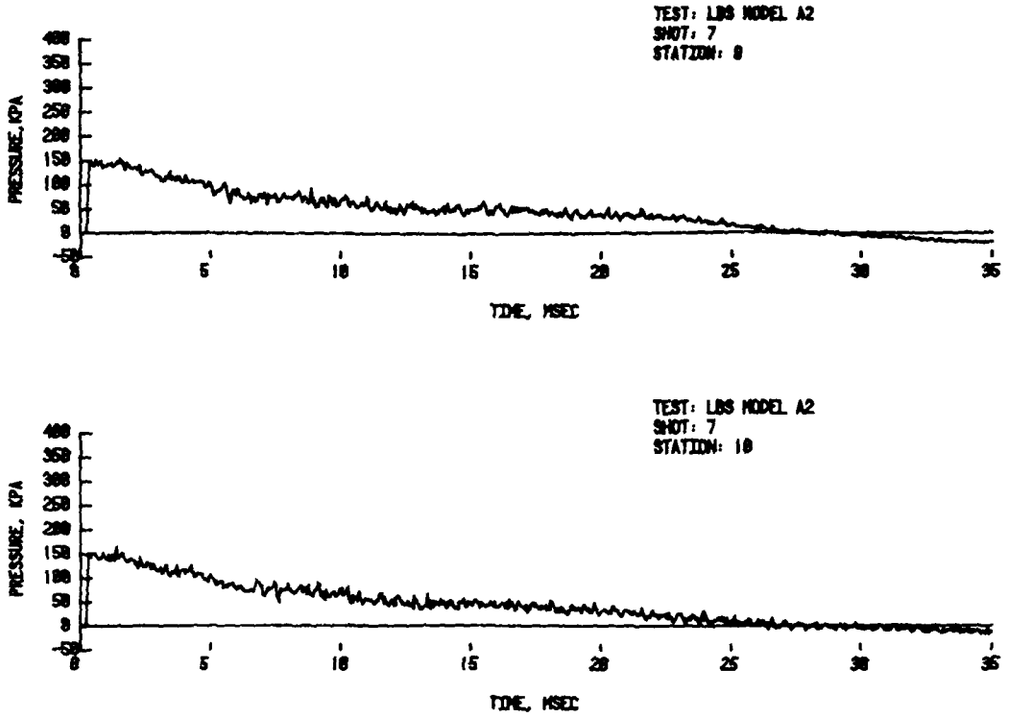

Figure 3. Typical Records for a Run (All Stations), (cont.)

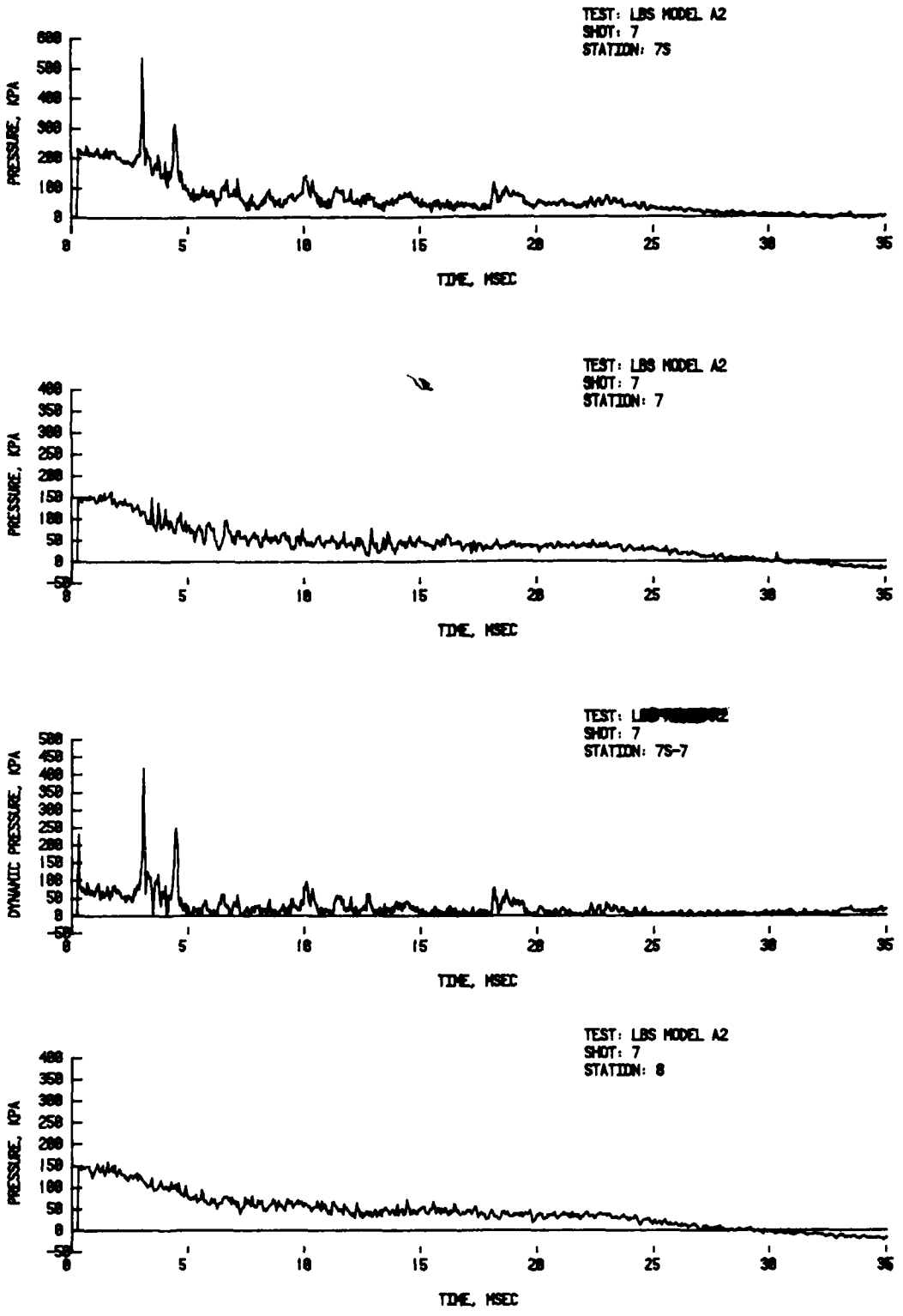

Figure 3. Typical Records for a Run (All Stations), (cont.)

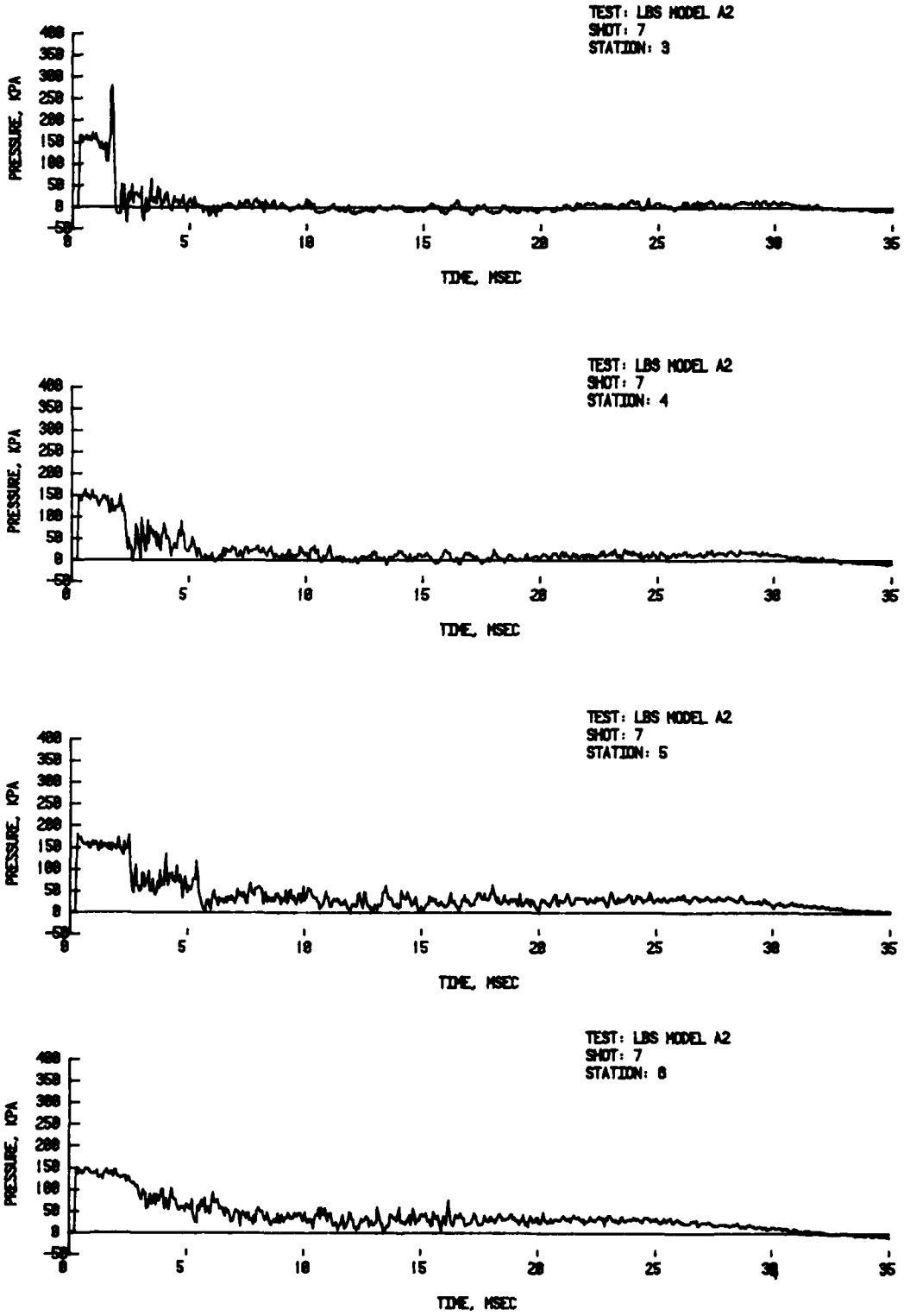

Figure 3. Typical Records for a Run (All Stations), (cont.)

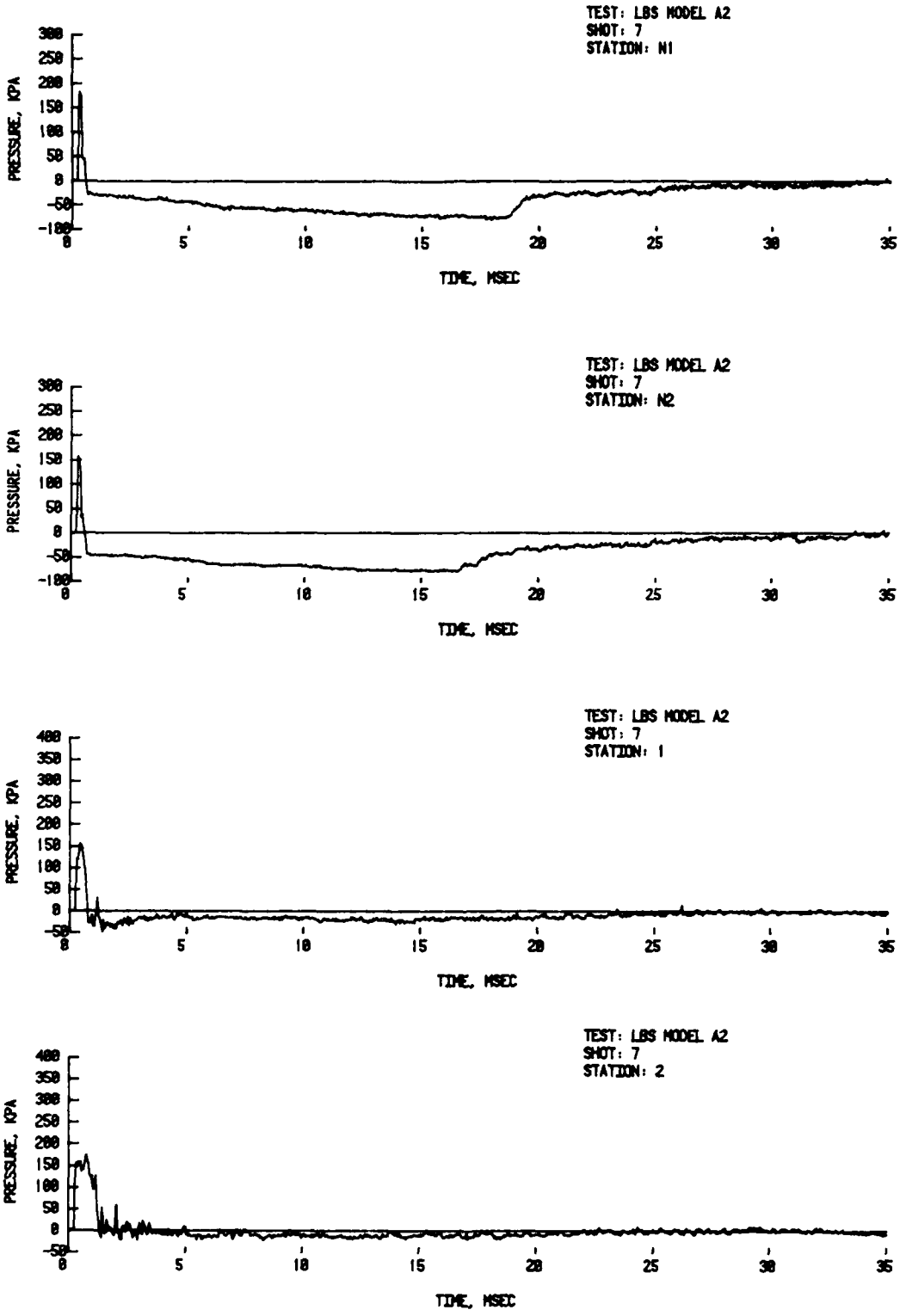

Figure 3. Typical Records for a Run (All Stations)

It may be observed that for the highest level Shots 21 and 22 the pressures measured are a bit higher than would be predicted, opposite to the trend for the lower level shots. With an applications bias in mind, the pressure measured here was the mean, gross level characteristic of the wave, which for these shots occurred some small time after the incident shock, unlike the earlier shots. Immediately behind the shock, flow properties should depend only on the shock Mach number, as indeed they do for Shots 21 and 22 also. The situation thus suggests that at the "Test Station-7" one is not observing the model tube's fully developed flow behavior for these highest pressure levels.

In Figure 3 we show pressures recorded over all the stations for a medium pressure run, Shot 7. It illustrates the experimental shock tube performance and a number of the wave processes occurring and propagating downstream. Attempts to follow individual and expected flow phenomena down the tube were not overly successful, due to complexity and lack of precise knowledge of the interactions occurring in the stepped driver.

In the traces, one typically sees, in the diverging section (Stations N1, N2) and for the first few stations (diameters) down the driven tube, the sharp rise in pressure with shock passage, then a steep decay as the backward-facing shock and a low pressure flow characteristic of jet overexpansion passes over the gage. The shock pressure is maintained for longer intervals as the shock advances downstream, ultimately taking on the desired decaying wave form at the Test Station 7 and following stations. A considerable amount of electrical and other noise is present in the traces. (Gages were not shock-mounted in the tube walls.) Possibly masked are true flow-induced fluctuations in the p/t histories. The sources and effects of various other waves in the flow will be discussed more fully in the computational sections.

1. Driver Temperatures During Pressurizing. As mentioned, experiments were performed to determine temperature changes in the driver during pressurizing, to see if the changes were significant and might cause departure from ideal shock tube operation. Three thermocouples were installed down the axis of the driver at positions labelled T2, T17, and T32, (inches back from diaphragm station) to place one near the diaphragm, one near mid-driver, and one near the inlet air orifice at the end wall, respectively. These were carried by a rod fastened to a thick plate at the diaphragm station used to seal off the driver, thus permitting a simulation of the pressurizing operation.

distribution in temperatures during the pressurizing, which was not entirely expected. Also, the stagnation probe at the test station was moved radially to observe effects of annular plate removal, and records for these will be shown.

B. Experimental Results

The run conditions achieved with the various diaphragms used are given in Table 1. A range of shock pressures from 3.1 - 31 psi (21-214 kPa) was obtained at the test station. The computed shock pressure (ratio) based on measured shock velocity and shock tables is also tabulated, as a check on gage accuracy and to note any significant departure from normal shock tube behavior.

TABLE 1: FLOW CONDITIONS

	Measured					From Measured U_s and Shock Tables
Shot #	P4/P1*	U_s (m/s)	$\Delta p2$* (kPa)	$\Delta p2$* (psi)	p2/p1*	p2/p1*
20	6.9	364	21	3.1	1.21	1.22
2	16	413	37	5.4	1.36	1.36
3	29	457	79	11	1.78	1.78
5	47	492	103	15	2.02	2.17
6	65	517	128	19	2.27	2.41
7	99	524	152	22	2.50	2.62
8	133	566	172	25	2.70	2.88
12	135	555	172	25	2.70	2.86
22	165	532	190	28	2.88	2.75
21	202	558	210	31	3.07	2.97

* p4/p1 - driver/driven pressure ratio
* Δ p2 - shock overpressure
* p2/p1 - pressure ratio across shock

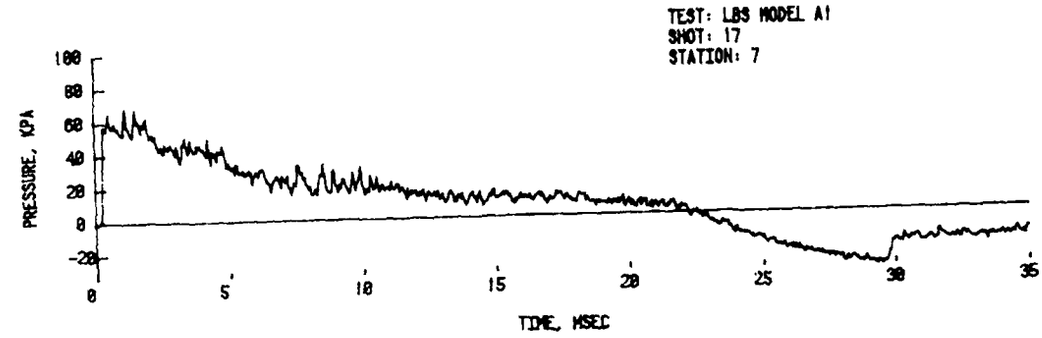

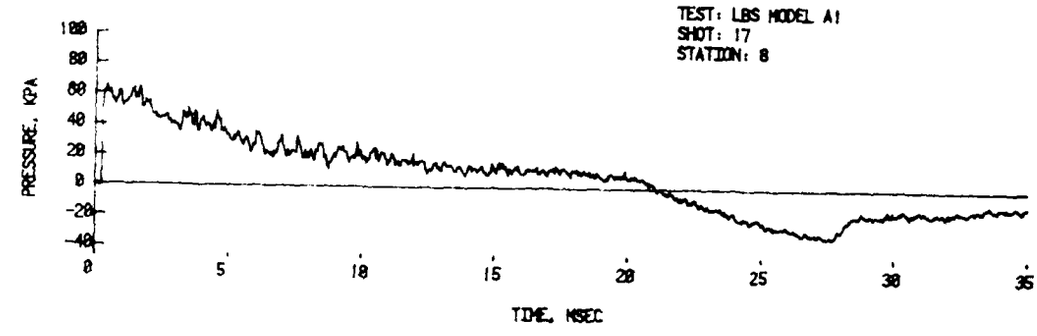

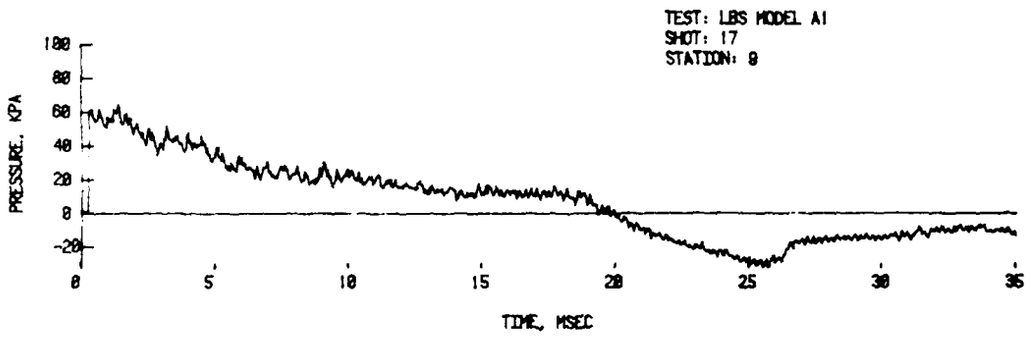

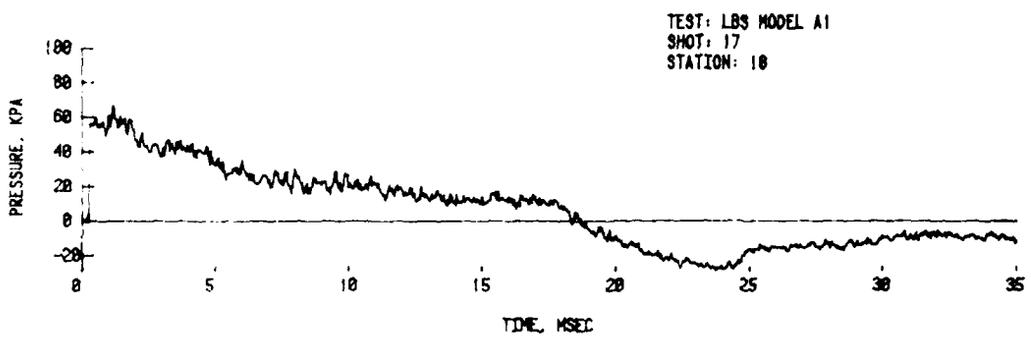

b. Low Level Shock Flow (cont.)

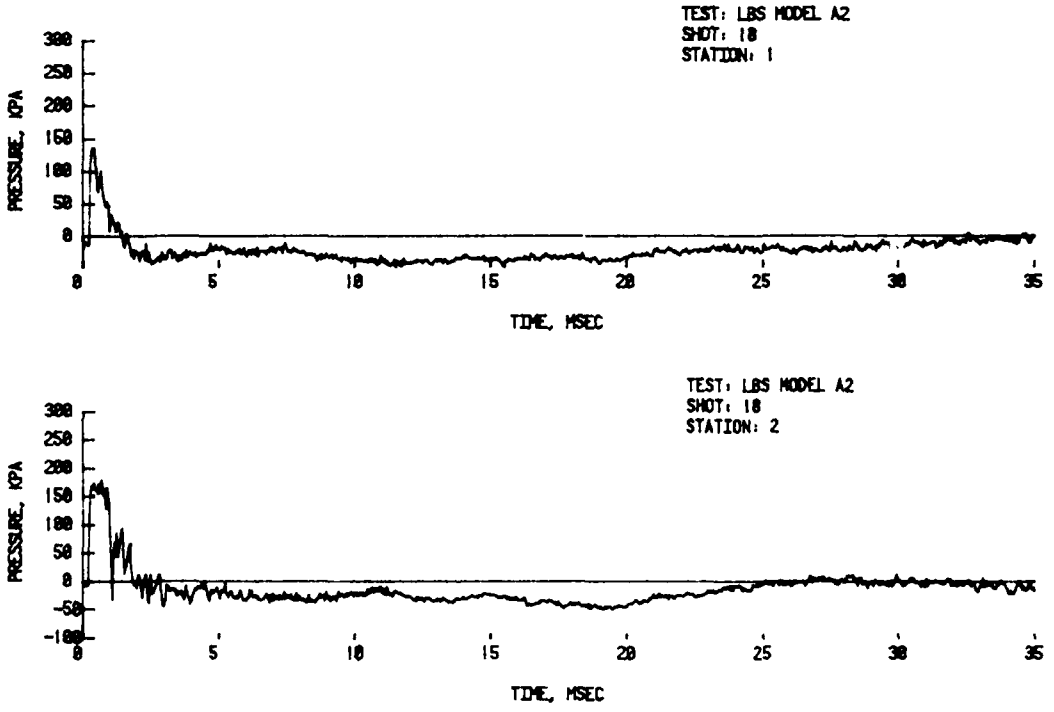

c. High Level Shock Flow

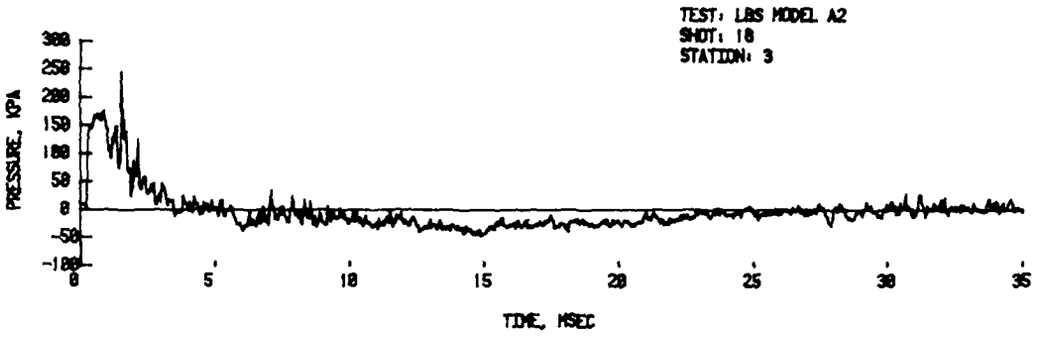

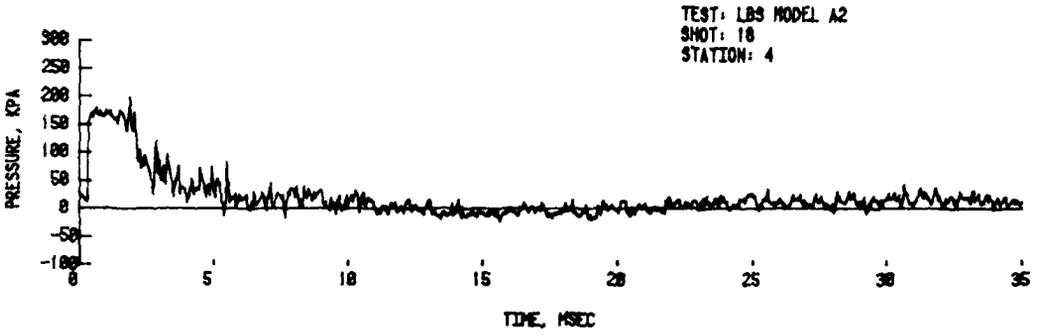

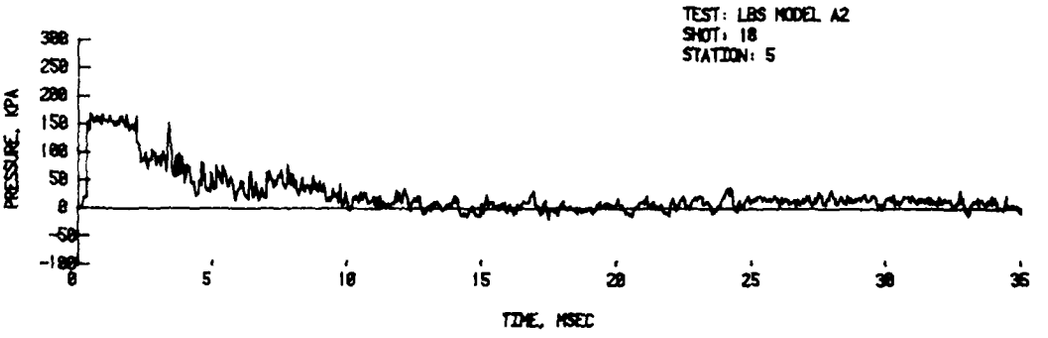

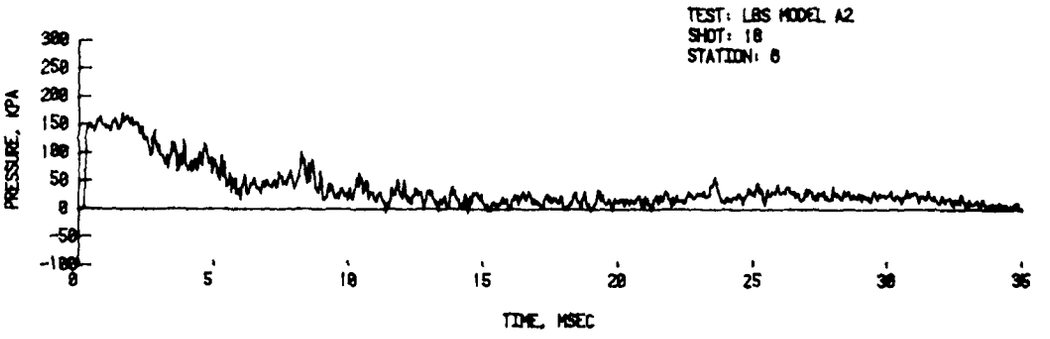

c. High Level Shock Flow (cont.)

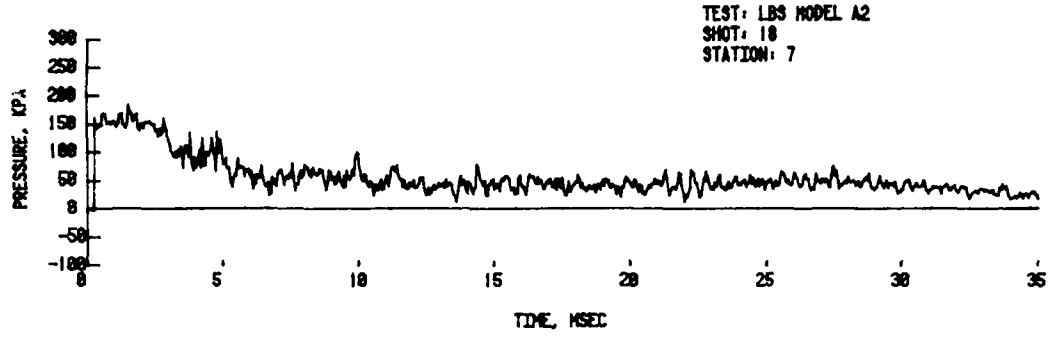

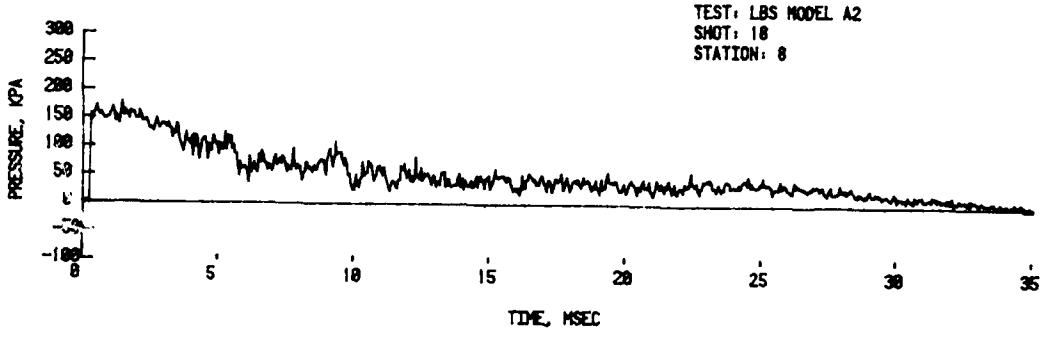

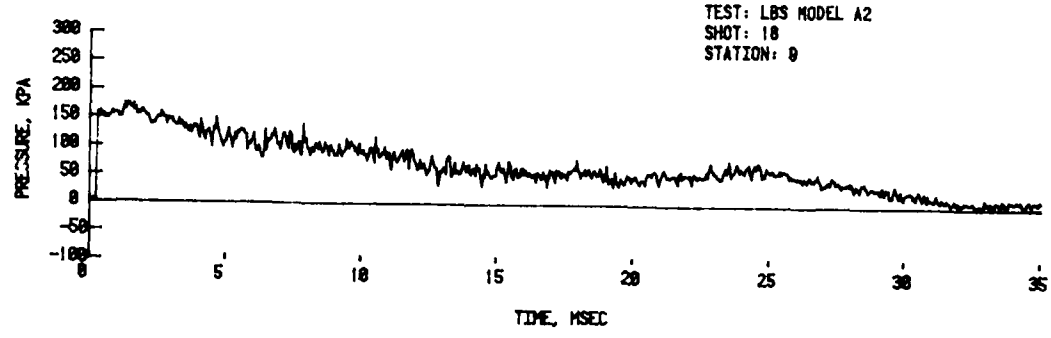

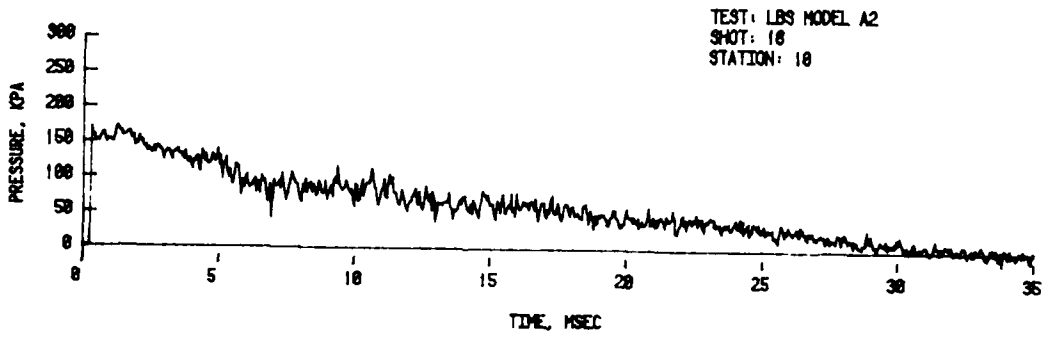

c. High Level Shock Flow (cont.)

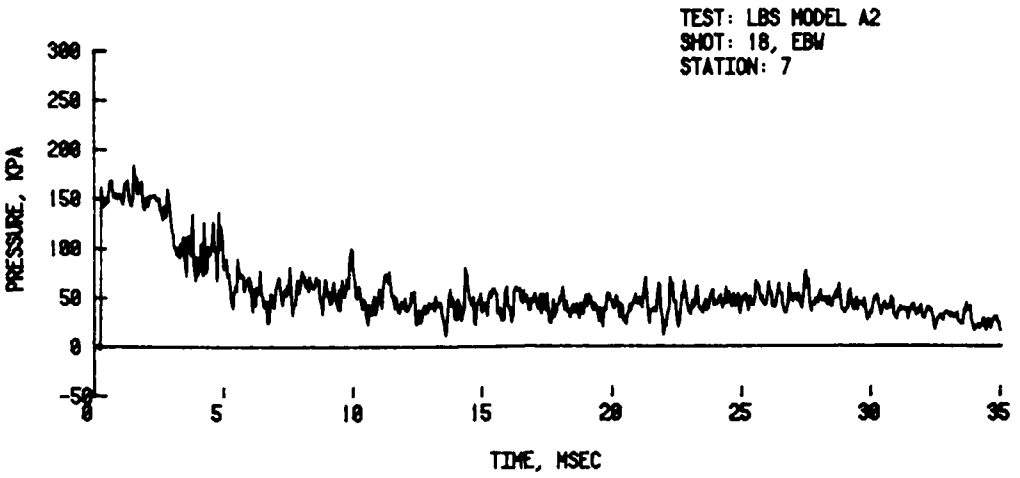

a. Detonator Burst of Diaphragm - Annulus Plate Out

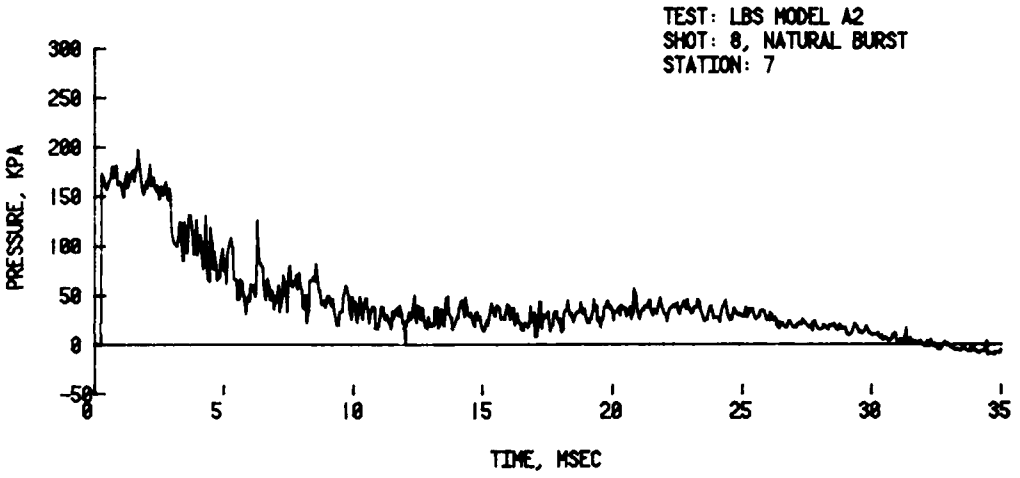

b. Natural Burst of Diaphragm - Annulus Plate Out

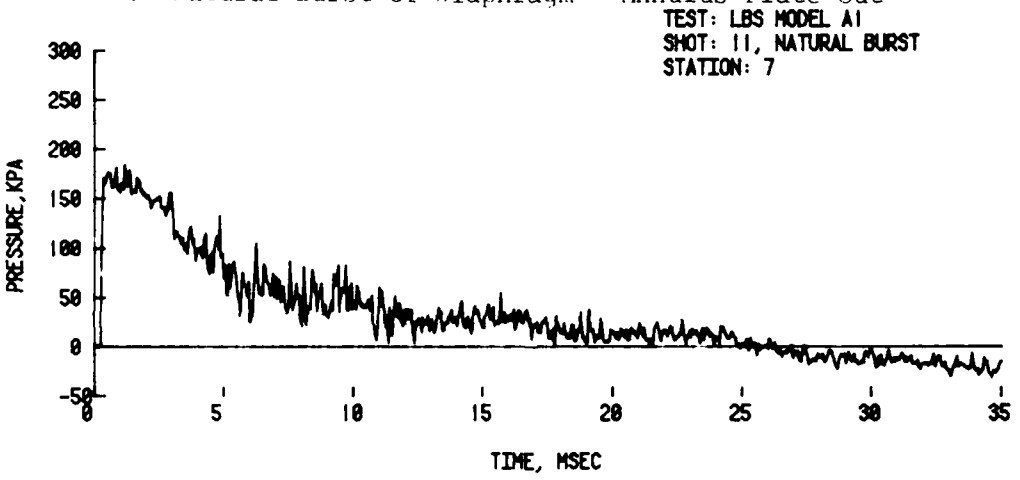

c. Natural Burst of Diaphragm - Annulus Plate In

Figure 8. Comparison of Shots

III. ONE-DIMENSIONAL COMPUTATIONAL MODELING

This section describes the one-dimensional computational study performed for modeling the two-dimensional axisymmetric experimental shock tube. The study involves computational simulations of related configurations, and results of the 1-D computational predictions for the 2-D axisymmetric experimental shock tube. All references to computations or calculations imply usage of the BRL Quasi-one-dimensional (Q1D) Code.

A. BRL Q1D Code

One of the basic research efforts at the Ballistic Research Laboratory (BRL) is to computationally model shock tube processes. The BRL Q1D Code is an adiabatic, inviscid eulerian computer algorithm adapted by BRL[3] for this purpose. There are many references which present good descriptions of the code's computer algorithm.[6,7] To summarize, the flow chart in Figure 9 illustrates the basic computational cycle in the BRL Q1D Code. As shown in the flow chart, the first step is to lay out a finite difference grid along the shock tube. The computational grid may be equidistantly partitioned along the tube length or cells may be clustered about a specified location utilizing the hyperbolic function incorporated in the code. Thus, a large number of grid points may be positioned where cross-sectional area changes occur. Typically, the number of spacial grid points varies from 100-1000.

Then, the initial conditions are set and normalized. The ideal gas equation of state, equation 1, and the Euler equations, equation 2, are applied to the shock tube where P = Pressure, γ is the ratio of specific heats, E = Total Energy/Volume, ρ = Density, U = Flow Velocity, A = Tube Cross-Sectional Area, T = Time, and X = Distance.

---

[6] *G. Coulter and others, "Experimental and Computational Modeling of Rarefaction Wave Eliminators Suitable for the BRL 2.44m Shock Tube," US Army Technical Report ARBRL-TR-02503, BRL, APG, MD, June 1983. (AD A131 894)*

[7] *A. Mark, "Computations of Shock Wave Target Interaction," US Army Technical Report ARBRL-TR-02538, BRL, APG, MD, December 1983. (AD B079 280L)*

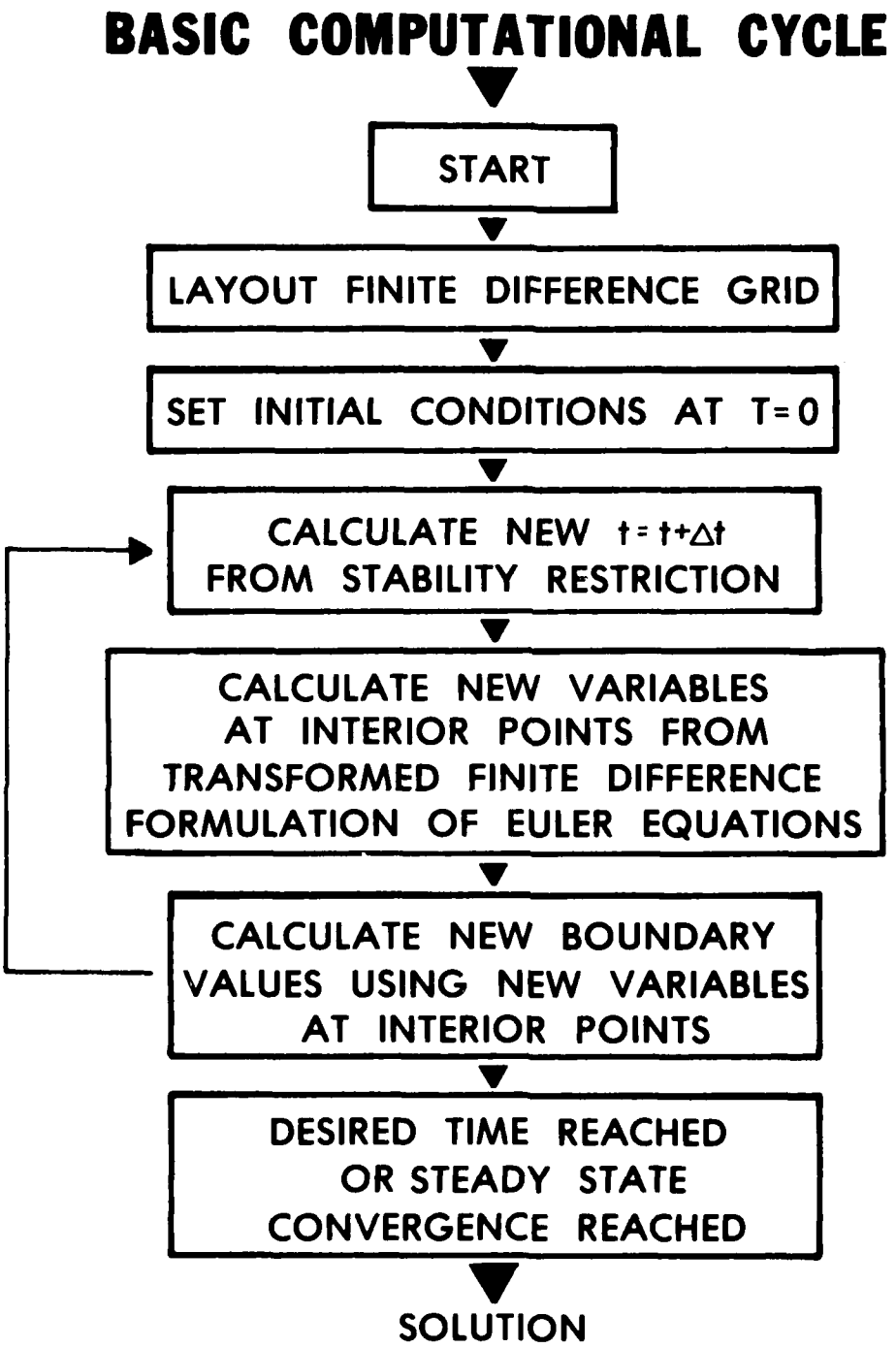

Figure 9. Basic Computational Cycle

$$P = (\gamma-1)\ (E - \tfrac{1}{2}\rho U^2), \tag{1}$$

$$\frac{\partial(\rho A)}{\partial t} + \frac{\partial}{\partial x}\ (\rho UA) = 0 \tag{2-a}$$

$$\frac{\partial(\rho UA)}{\partial t} + \frac{\partial}{\partial x}\ (\rho U^2 + P)A\ - P\ \frac{\partial A}{\partial x} = 0, \text{ and} \tag{2-b}$$

$$\frac{\partial\ (EA)}{\partial t} + \frac{\partial}{\partial x}\ uA(E + p) = 0, \tag{2-c}$$

New variables at interior points are calculated from a finite difference formulation of the transformed Euler equations. The Euler equations for conservation of mass, momentum, and energy per unit volume are solved in differential form for the field variables density, pressure, temperature, total energy, and a one-dimensional component of flow velocity using finite differencing techniques attributed to Beam and Warming.[8]

New boundary values are calculated for the open end of the shock tube using the new variables at the interior points and conditions suggested by characteristic theory. New boundary values are calculated for the closed end of the tube using image points and reflection principles. Then the computational cycle is repeated until the desired time is reached, or until some convergence criterion for a steady state is satisfied.

One-dimensional computational modeling has its advantages and disadvantages. Advantages include 1) inexpensive to run, 2) capability to perform parametric studies quickly, and 3) usefulness for obtaining good engineering approximations to a wide variety of flow problems. The obvious disadvantage is that one-dimensional analysis is necessarily an approximation. No real flow exists that is truly one-dimensional. Further, there are many problems which are not adequately represented by one-dimensional analysis, for example, flow from a nonaxisymmetric shock tube.

However, the axisymmetry of the experimental shock tube and related configurations leads one to expect good results from a one-dimensional analysis of their flow properties.

---

[8] *R. M. Beam and R. F. Warming, "An Implicit Factored Scheme for the Compressible Navier-Stokes Equations," AIAA J.16, 393-402, April 1978.*

B. Computational Modeling of Related Configurations

First, the results of computationally modeling related configurations are presented. This section is included because, referring to Figure 1, the 1-D computational model of the experimental shock tube is complicated with various area changes. In order to understand the individual effects of these area changes, and to establish the credibility of the BRL Q1D Code, similar area changes are modeled separately and compared to experiments where possible. The area changes consist of A) a converging nozzle, B) a driver section with complicated area changes, and C) a diverging nozzle.

For the converging nozzle, experimental and computational data reported by Gottlieb are used to substantiate the accuracy of the BRL Q1D Code. The computational algorithm employed by Gottlieb is the Random Choice Method (RCM).[9-10] Unlike finite difference schemes, such as the Beam and Warming scheme in the BRL Q1D Code, viscosity terms are incorporated in the governing equation of motion to deal with the presence of discontinuities. In the RCM, shock waves and contact surfaces are inherently discontinuous, occupying an unspecified position between two grid points in the flow field. To first order accuracy the location of such discontinuities is not exact, but their average positions are. Furthermore, numerical viscosity effects and truncation error accumulation are not inherent in the RCM algorithm. Thus, the RCM algorithm is considered a good computational method for validation of the BRL Q1D Code.

A comparison of Gottlieb's experimental and RCM-generated data[11] with the BRL Q1D Code-generated data for the converging nozzle reveals excellent agreement, Figure 10. In Figure 10, the large decays in pressure are caused by the reflection of the rarefaction wave, created upon burst of the diaphragm, from the closed end of the tube. The rarefaction wave travels into the driver sec-

---

[9] *J. Glimm, "Solution in the Large for Nonlinear Hyperbolic Systems of Equations," Communications in Pure and Applied Mathematics, Vol. 18, 679-715, 1965.*

[10] *T. Saito and I. I. Glass. "Application of Random Choice Method to Problems in Shock and Detonation Wave Dynamics," UTIAS Report No. 240, University of Toronto Institute for Aerospace Studies, Downsview, Ontario, Canada, October 1979.*

[11] *Private Communication from Dr. J. J. Gottlieb, University of Toronto Institute for Aerospace Studies to Dr. A. Mark, Ballistic Research Laboratory, March 1983.*

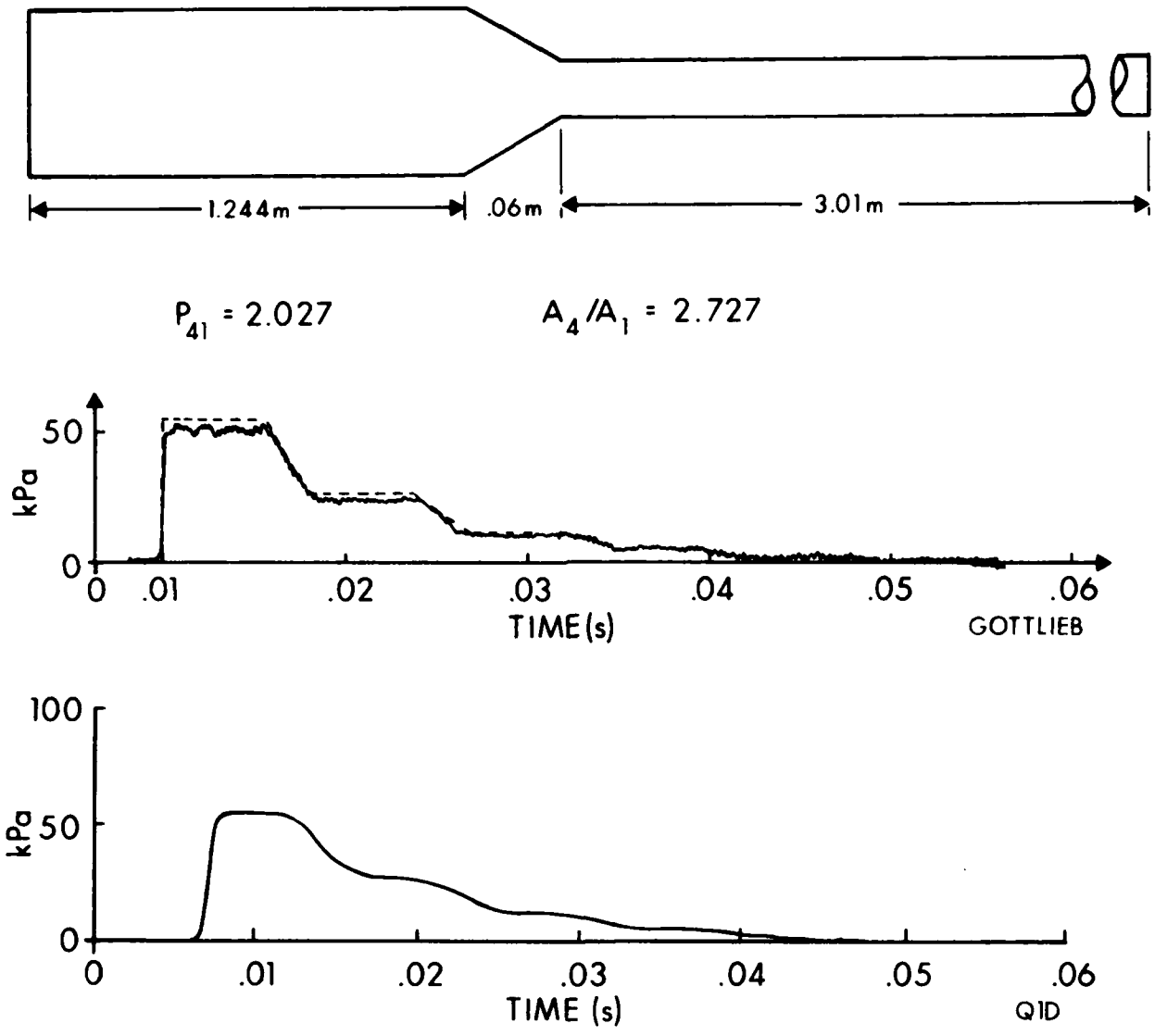

Figure 10. Converging Nozzle Shock Tube

tion, reflects from the closed end, and interacts with the converging nozzle such that the rarefaction wave is partly transmitted and partly reflected. The transmitted rarefaction wave overtakes the initial shock, causing a decay in pressure. The reflected rarefaction wave cycles again in the driver section in the same manner as the initial rarefaction wave. From Figure 10, four pressure drops are noted which correspond to four cycled interactions of the initial rarefaction wave with the converging nozzle.

In another report,[12] Gottlieb presents RCM-generated results for a shock tube with area changes in the driver section. Again, the BRL Q1D Code data agrees remarkably well with Gottlieb's results, Figure 11. Figure 11 shows fluctuations or dips in the pressure-time histories. These fluctuations result from the interaction of the rarefaction wave with the parabolic area changes. As the rarefaction wave moves through the convergent part of a parabolic area change, a reflected rarefaction wave is produced. As the rarefaction wave moves through the divergent part of a parabolic area change, a reflected compression wave is produced, which follows the reflected rarefaction wave. These reflected waves appear as V-shaped fluctuations, or dips in the pressure-time histories. Gottlieb and others note the existence of head losses for this and other configurations where severe area contractions are present in the driver. Generally, head losses are largest for sudden area expansions and contractions. The losses in sudden area changes are explained in terms of the vortex formation that occurs when flow separation takes place. Energy must be supplied to maintain the vortex motion against the action of viscous forces. Computationally, the inclusion of head losses cause a larger decay rate and a lengthening of the positive phase duration. Head losses become extremely significant for severe area contractions and high local velocities.

As a final check on the BRL Q1D Code's ability to model area changes a diverging nozzle configuration is examined. Experimental data for a diverging nozzle is obtained from a report by Coulter and Bertrand.[13] Once again, the BRL QID Code does an acceptable job of predicting the experimental results, Figure 12. An interesting feature of the diverging nozzle pressure-time history is the spike at the beginning of the waveform. The spike is attributed to complex wave interactions that occur in the vicinity of the exit of the diverging nozzle. An exact and complete analysis of the spike formation process is beyond the scope of this study; therefore, it will be reported on at a later date.

---

[12] *J. J. Goettlieb and others, "Use of Perforated Plates in the Driver Section of the BRL 8-ft. Shock Tube to Produce Simulated Blast Waves with Decaying Overpressures," 1st report, 15 March 1983, 2nd report 31 March 1983, 3rd and final report 7 April 1983. University of Toronto Institute for Aerospace studies, Ontario, Canada, M3H 5T6.*

[13] *George A. Coulter, "Shock Pressure Increase in Convergent Ducts," US Army BRL Memorandum Report No. 1625, BRL, APG, MD, January 1965 (AD 463927).*

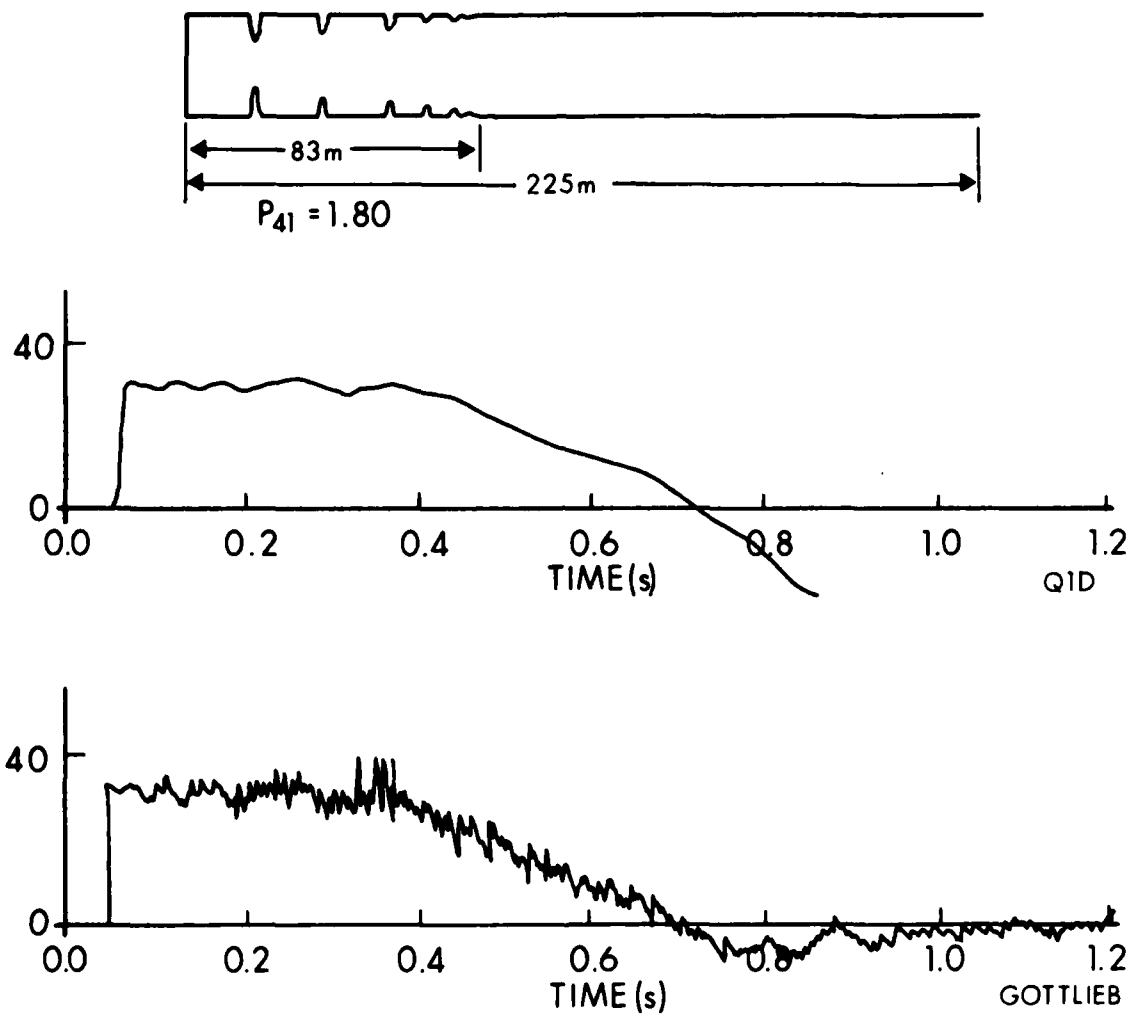

Figure 11. Multiple Area Changes in Driver Shock Tube

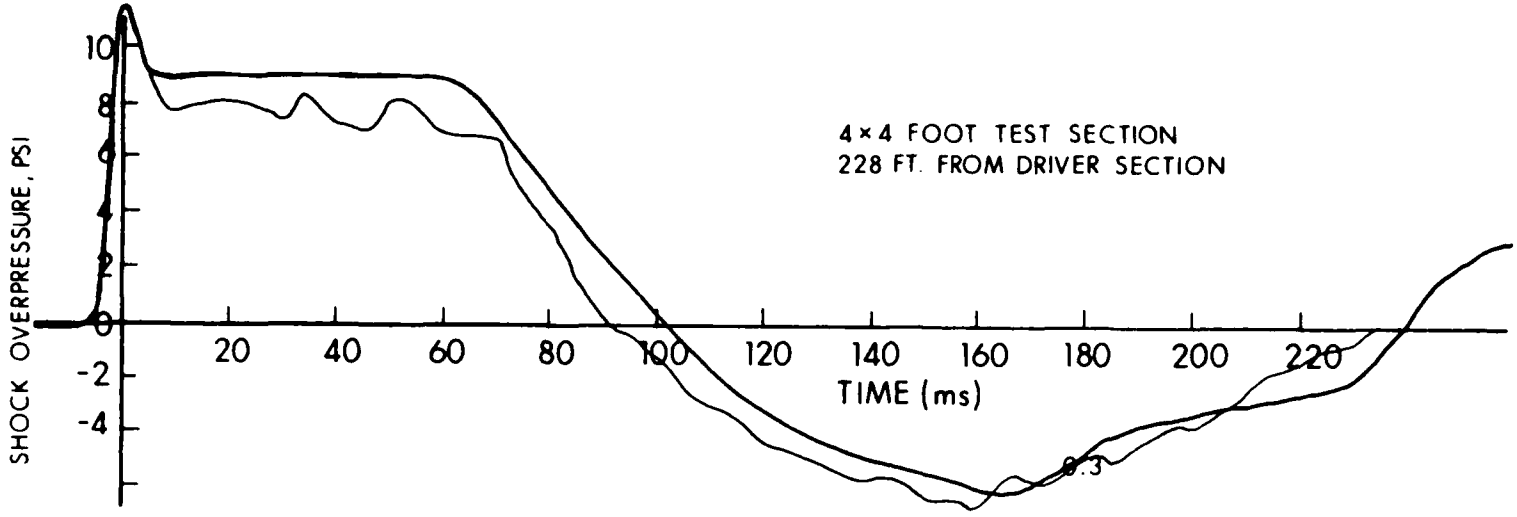

Figure 12. Diverging Nozzle Shock Tube

To recapitulate, the BRL Q1D Code results for the individual area changes compare favorably with experimental and computational counterparts. In anticipation of the next section, which deals with the combined effects of similar area changes in the experimental shock tube, one expects similar waveform characteristics.

C. Results of BRL Q1D Computations for 2-D Axisymmetric Experimental Shock Tube

The 1-D computational equivalent of the axisymmetric experimental shock tube is depicted in Figure 1b. The 1-D computational model preserves the experimental shock tube's cross-sectional areas and lengths. Thus, the computational model has a stepped driver, a converging-diverging nozzle and a long driven section.

Furthermore, the initial conditions noted for the experimental runs were used as input to the BRL Q1D Code, Table 1. Using the 1-D computational model and the initial conditions as input, the BRL Q1D Code generates pressure-time histories. The pressure-time histories become more familiar through an examination of the general characteristics of the computational waveforms and parametric studies of the pressure-time histories.

The general characteristics of the pressure-time histories at the test station are a sharp increase in pressure, the shock arrival, and a subsequent decay. The decay typically shows superimposed fluctuations. The fluctuations result when the rarefaction wave, produced upon breaking the diaphragm, propagates from the diaphragm location into the driver. As the rarefaction wave moves through convergent area changes (stepped driver), reflected rarefaction waves are produced which move in the opposite direction, following the blast wave front. These reflected rarefaction waves show up as small pressure drops in the pressure-time histories. Also, the waveform shows a significant pressure drop within the decaying signature. This large gradient is caused by the reflection of the rarefaction wave from the closed end of the shock tube. The computational and experimental pressure-time histories for lower driver pressures (Figures 16a through d) show spikes at the beginning of the decay. As stated earlier, this effect is directly related to the presence of the diverging nozzle. At the highest driver pressure, the waveform (figure 16c) shows an abrupt pressure drop which is caused by the arrival of a backward facing shock at the test station.

The computational parametric studies performed for the shock tube involve: A) temperature effect of pressurization, B) heated versus unheated driver, and C) diaphragm blockages.

As discussed in the experimental section, temperature changes in the driver are recorded during pressurizing for simulated shots over a range of driver pressure. One temperature distribution recorded at diaphragm "burst" is input to the BRL Q1D Code to see if any changes occur in the computationally generated pressure-time histories. No significant changes are caused by the temperature distribution. Therefore, the temperature effect, caused by pressurization, is concluded to be negligible for such shots and not a source of discrepancies between the experimental and computational records. The temperature effect would become more significant at higher pressures; however, the

Shots 5 and 6, Figures 16d and e, represent medium pressure shots; driver/driven pressure ratios are 47 and 65. A common characteristic of these shots is the removal of the annulus plate from the experimental shock tube to allow mass entrainment. Mass entrainment, particularly with increasing driver pressures sustains the positive phase pressure level. Computationally, the mass entrainment is not accounted for; therefore in Figures 16a and b, the pressure level the BRL Q1D Code predicts for the flow behind the shock wave is lower than the levels recorded experimentally. However, the comparison of trends in the traces due to rarefaction waves is in satisfactory agreement. Also, at earlier times the pressure-time histories agree extremely well, except for small discrepancies. The small discrepancies are attributed to experimental phenomena, such as Mach reflections and possibly some spike formation in Shot 5.

Shot 7 and 12, Figures 16f and g, represent high pressure shots; driver/driven pressure ratios are 99 and 135. Shot 7 is performed with the annulus out, thus entraining mass, while Shot 12 is performed with the annulus in. The discussion concerning mass entrainment for Shots 5 and 6 also applies to Shot 7. Upon comparing the experimental and computational pressure-time histories for the two shots, one notes the same characteristics in both cases. The computationally predicted pressure levels at early times are greater than the experimental levels. This implies that head losses, discussed earlier, and other types of losses (diaphragm, friction, heat transfer, etc.) are significant experimentally and should be accounted for computationally. Also, as described in the experimental section, diaphragm blockage effects are significant for these high pressure level shock tube runs. For Shot 7, the difference in pressure levels is not too great and the trends due to rarefaction waves agree. However, for Shot 12, the pressure levels are significantly different and the decay trends disagree. The comparison for Shot 12 is unsatisfactory, but by computationally modeling losses, currently under development, it is believed the comparison could be improved. The computational losses should lower the early pressure levels and lengthen the positive phase duration, thus providing a better match to the experimental data.

Shot 23, Figure 16h is a reiteration of Shot 12. However, instead of computationally modeling the diaphragm blockage from estimates (Shot 12), the diaphragm blockage is alleviated as described in the experimental section. A comparison of Shot 12 and Shot 23 indicates a much better experimental/computational match for Shot 23. This implies the diaphragm blockage is probably not accurately modeled and/or experimentally determined for Shot 12. Furthermore, Shot 23 is performed with the annulus out, thus entraining mass. This effect is evident in the longer positive phase duration.

Finally, Shot 21 represents the highest pressure level shock tube run (PRAT = 202). Again, as seen in the waveform match before 5 milliseconds, Figure 16i, losses are significant experimentally and are not accounted for computationally. The arrival of the backward-facing shock is captured within one half millisecond. The discrepancy after 5 milliseconds between the waveforms is attributed to mass entrainment which is not computationally modeled.

In Fig. 17 we exhibit the overall performance of the LBS model and its comparison with the quasi-1D calculations. Other available data from the

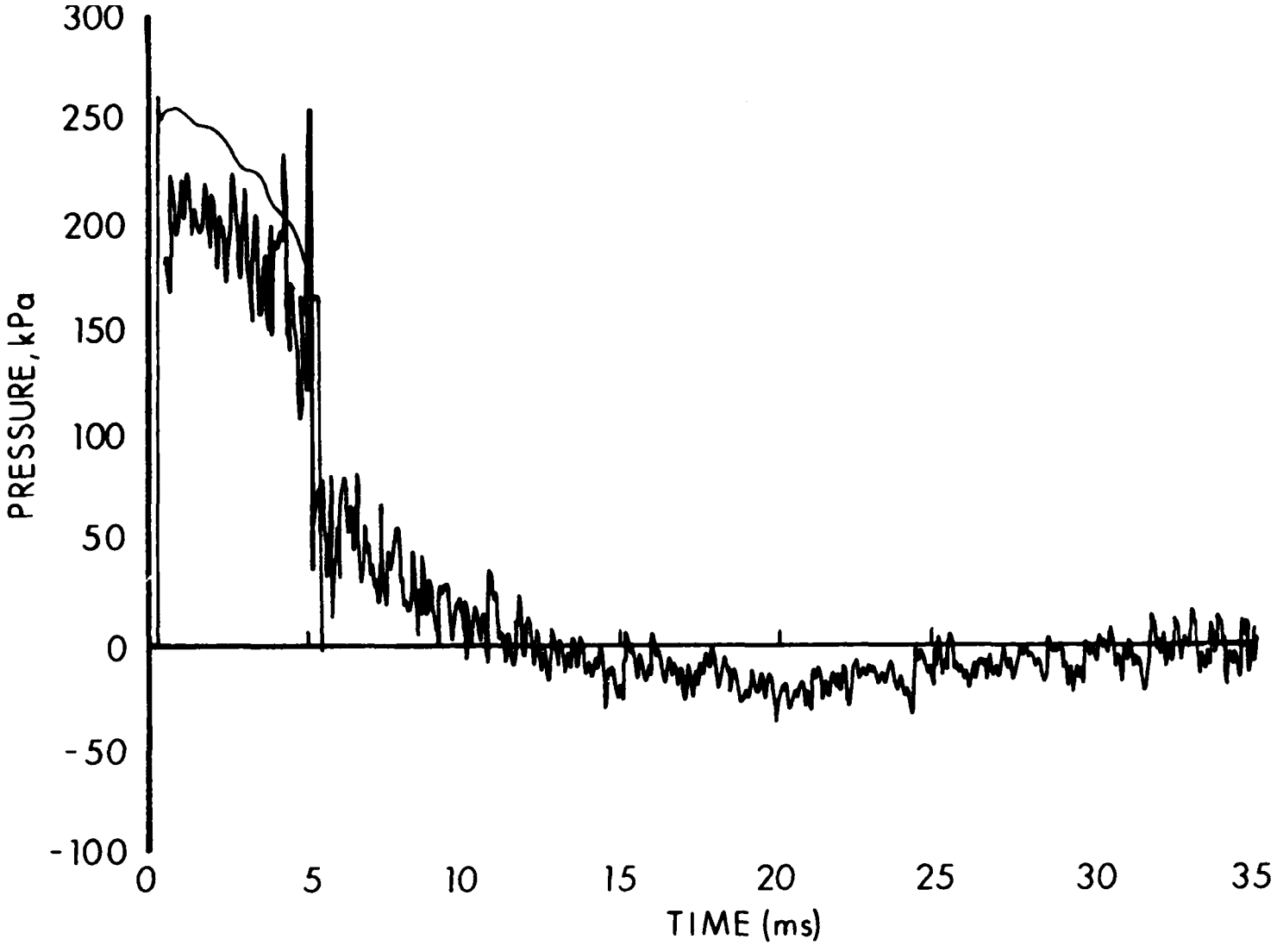

i. P-t Computational/Experimental Comparison, Shot 21

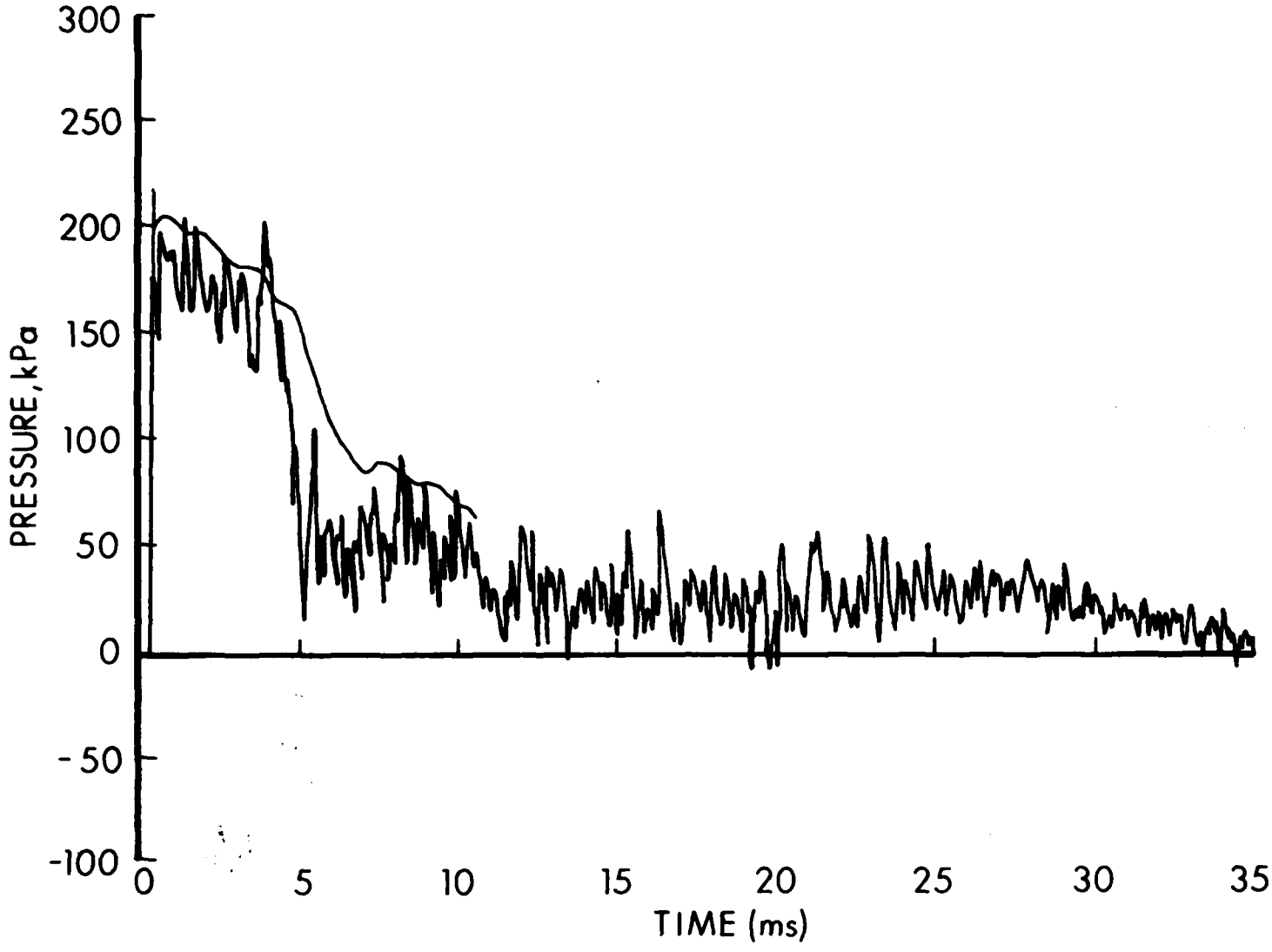

h. P-t Computational/Experimental Comparison, Shot 23

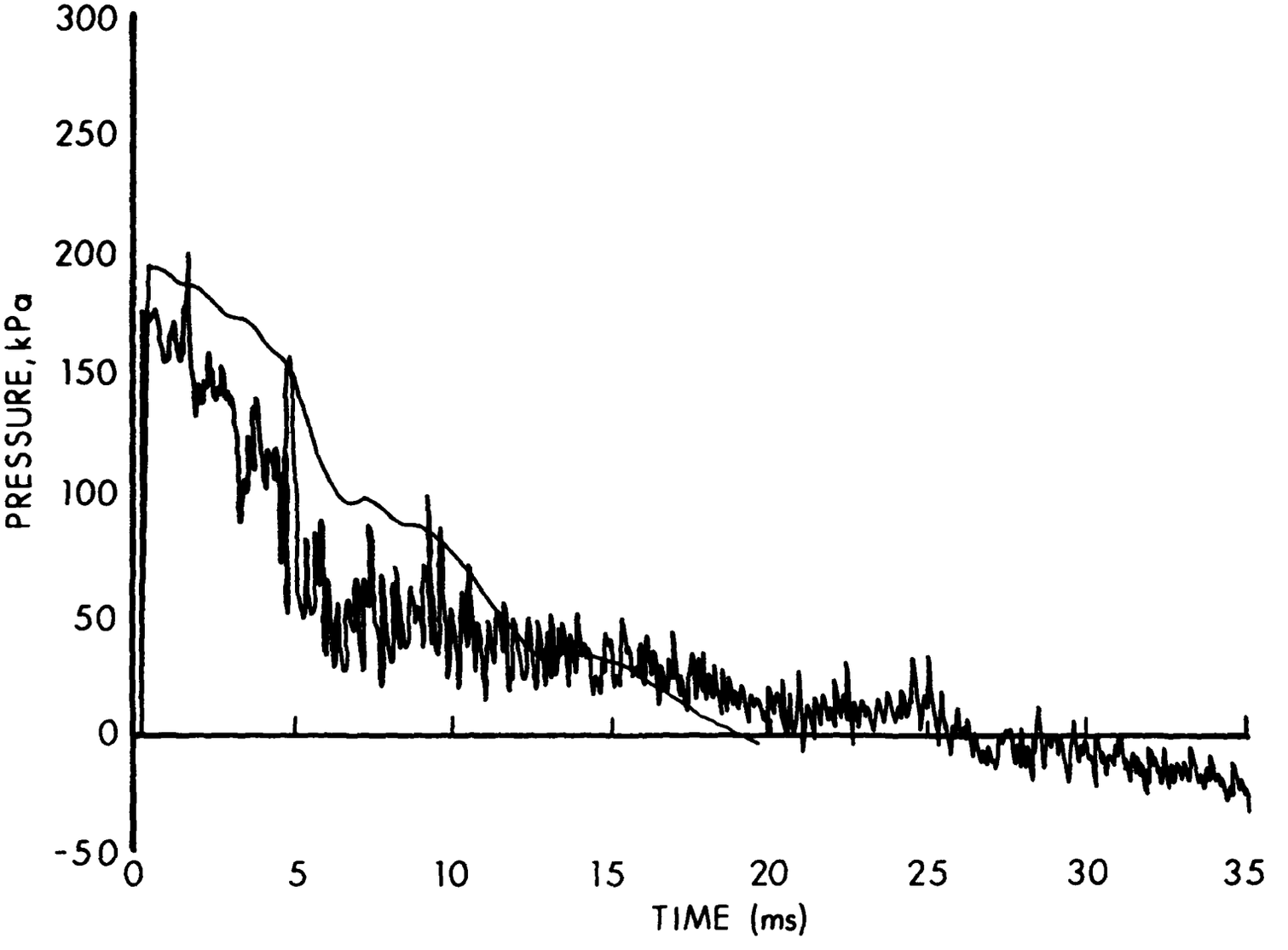

g. P-t Computational/Experimental Comparison, Shot 12

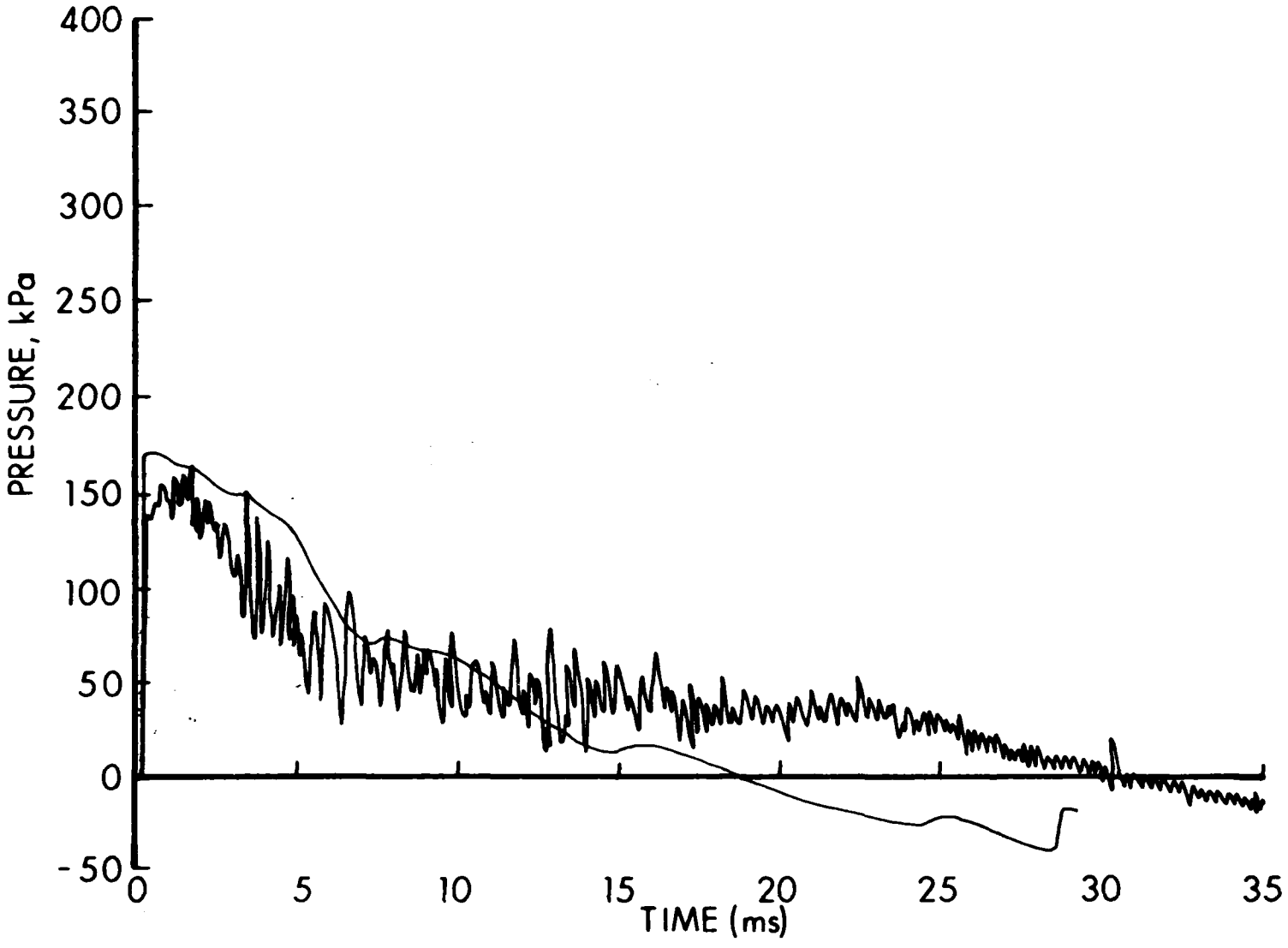

f. P-t Computational/Experimental Comparison, Shot 7

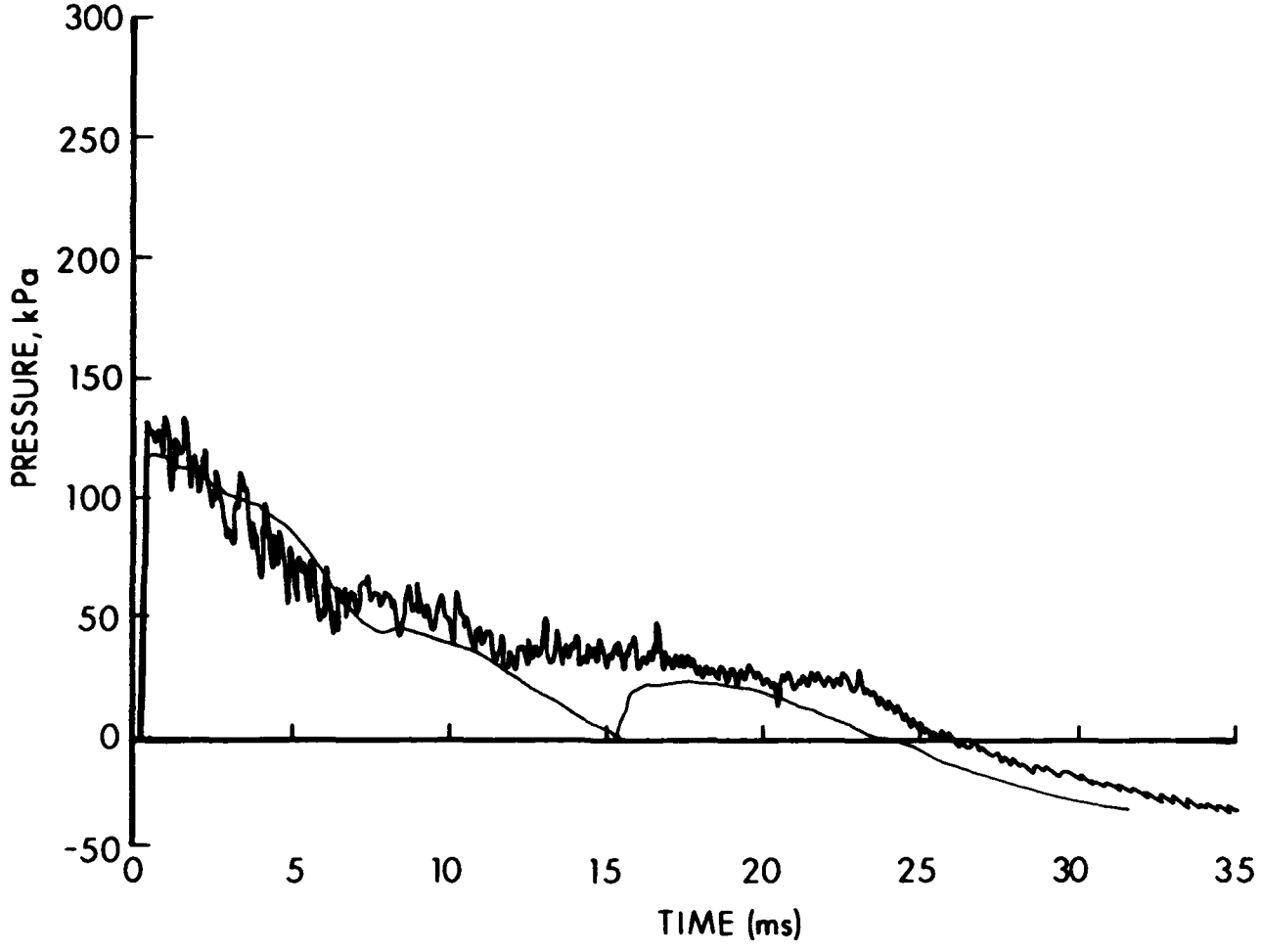

e. P-t Computational/Experimental Comparison, Shot 6

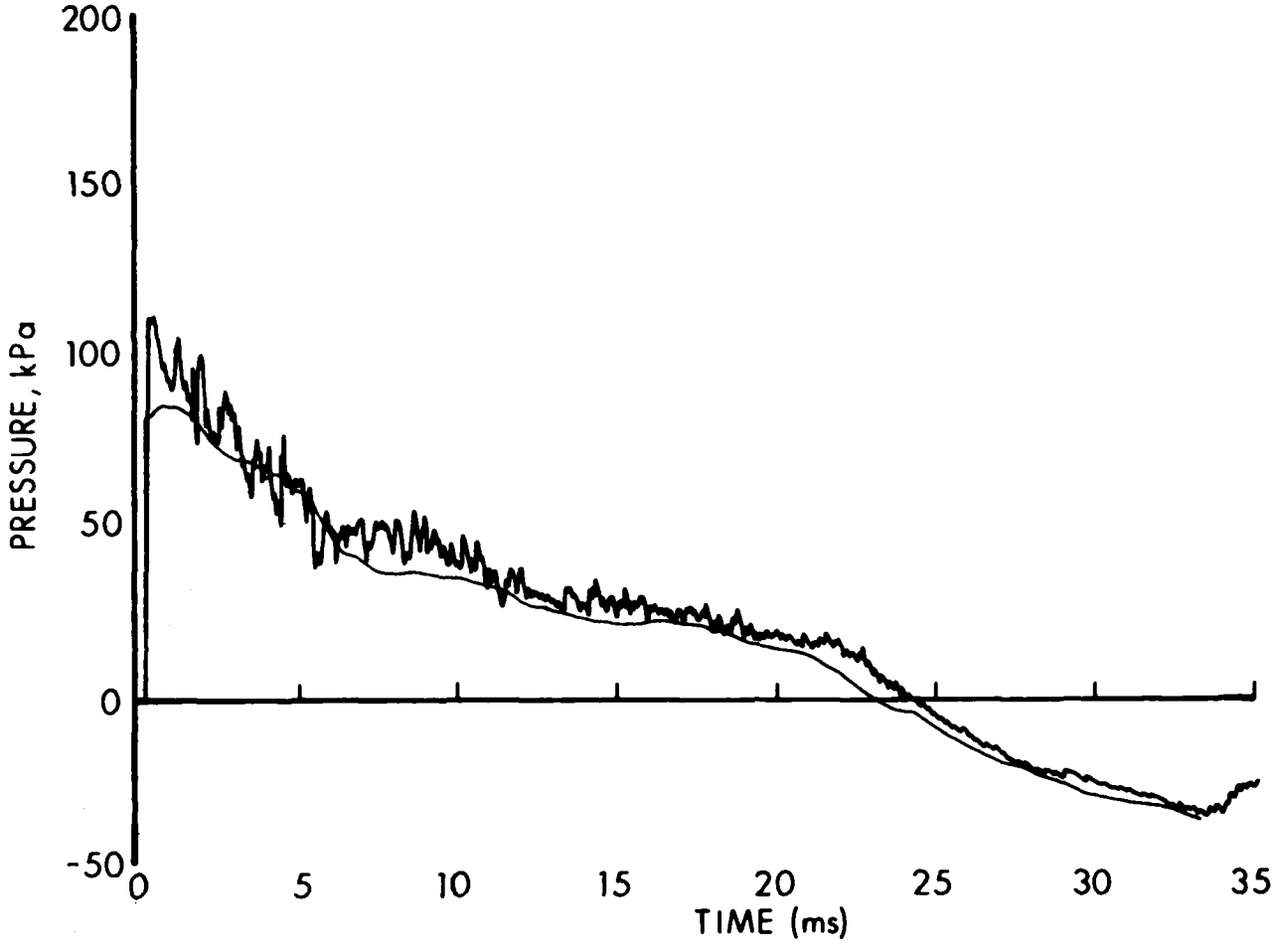

d. P-t Computational/Experimental Comparison, Shot 5

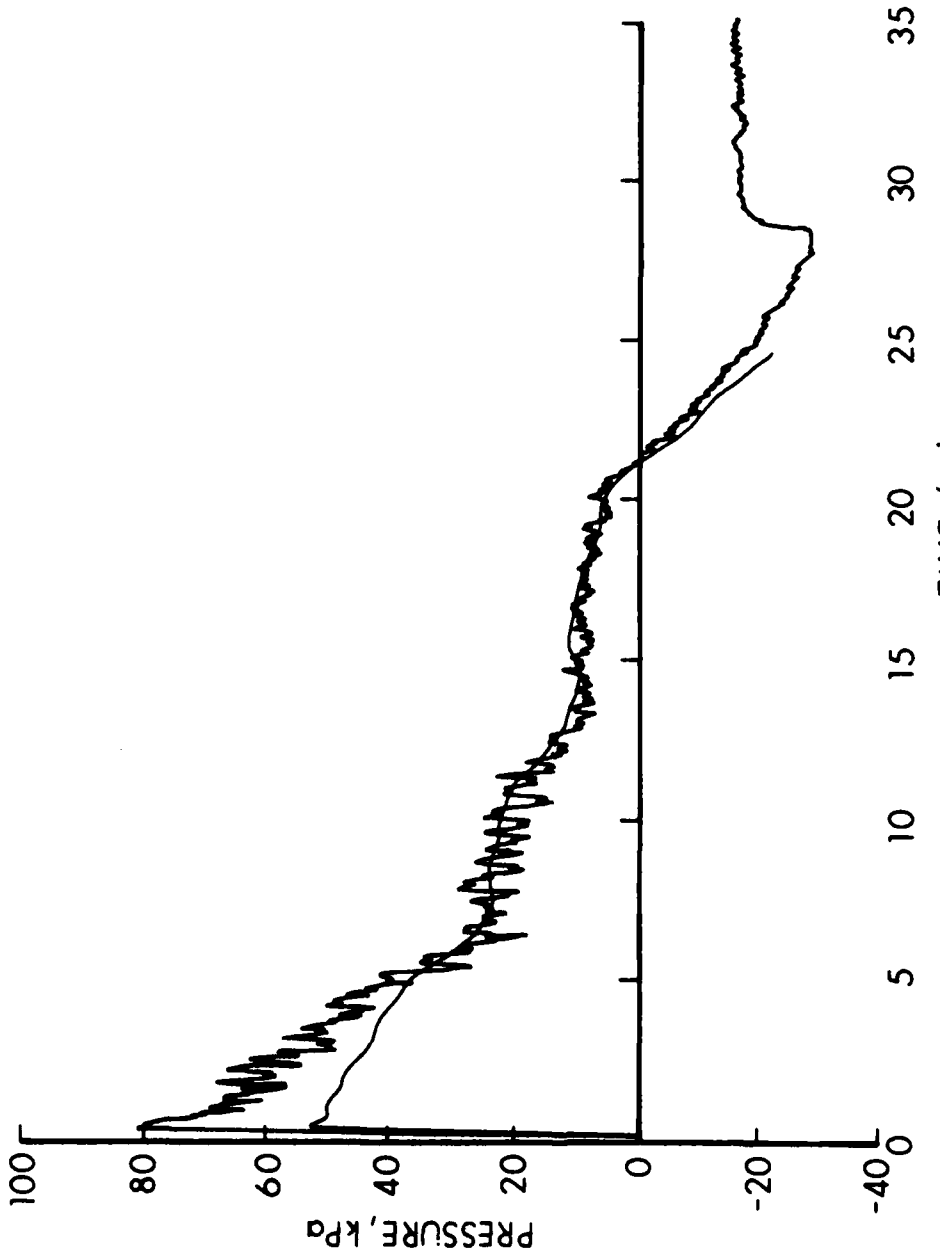

c. P-t Computaticnal/Experimental Comparison, Shot 3

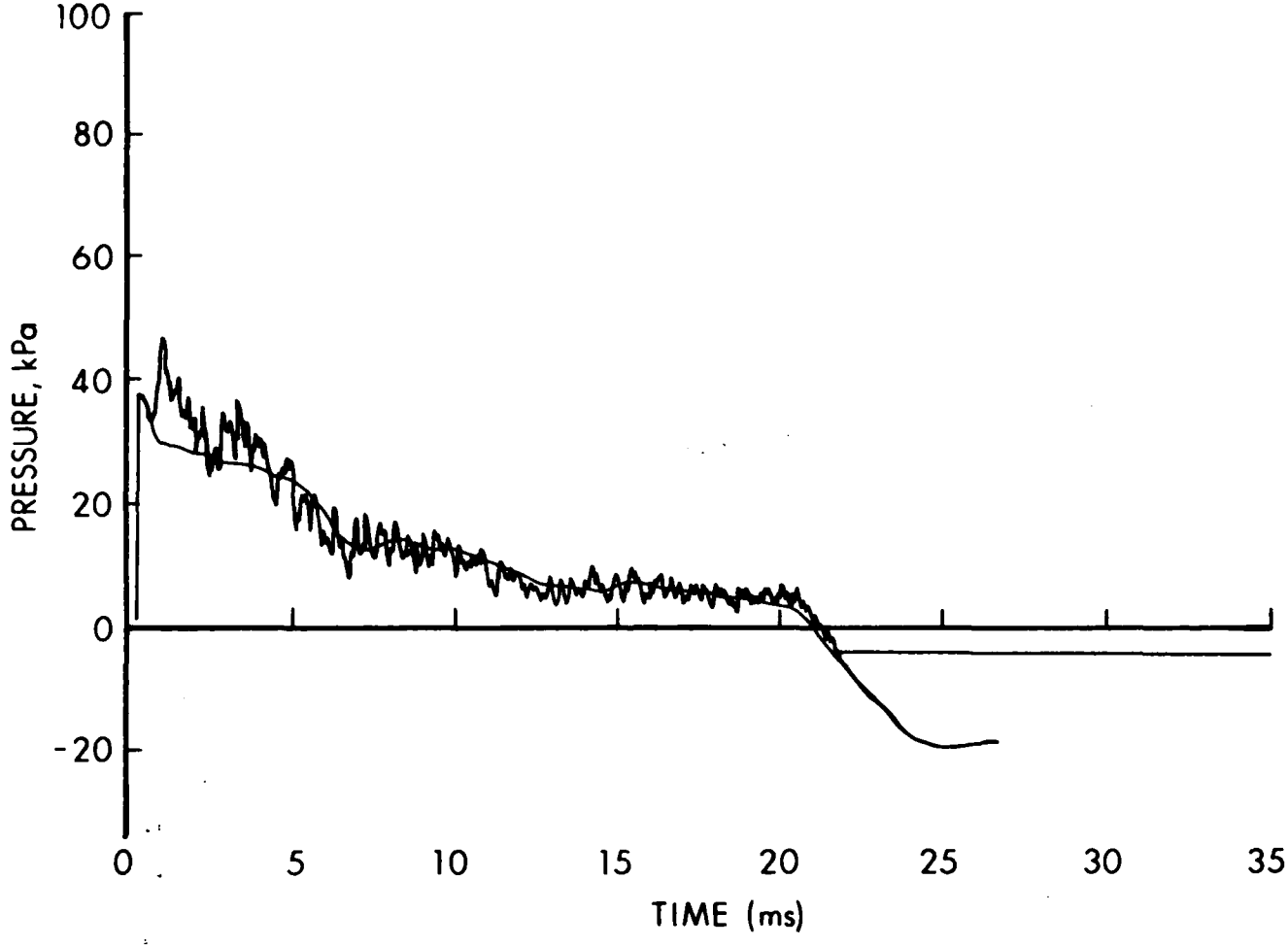

b. P-t Computational/Experimental Comparison, Shot 2

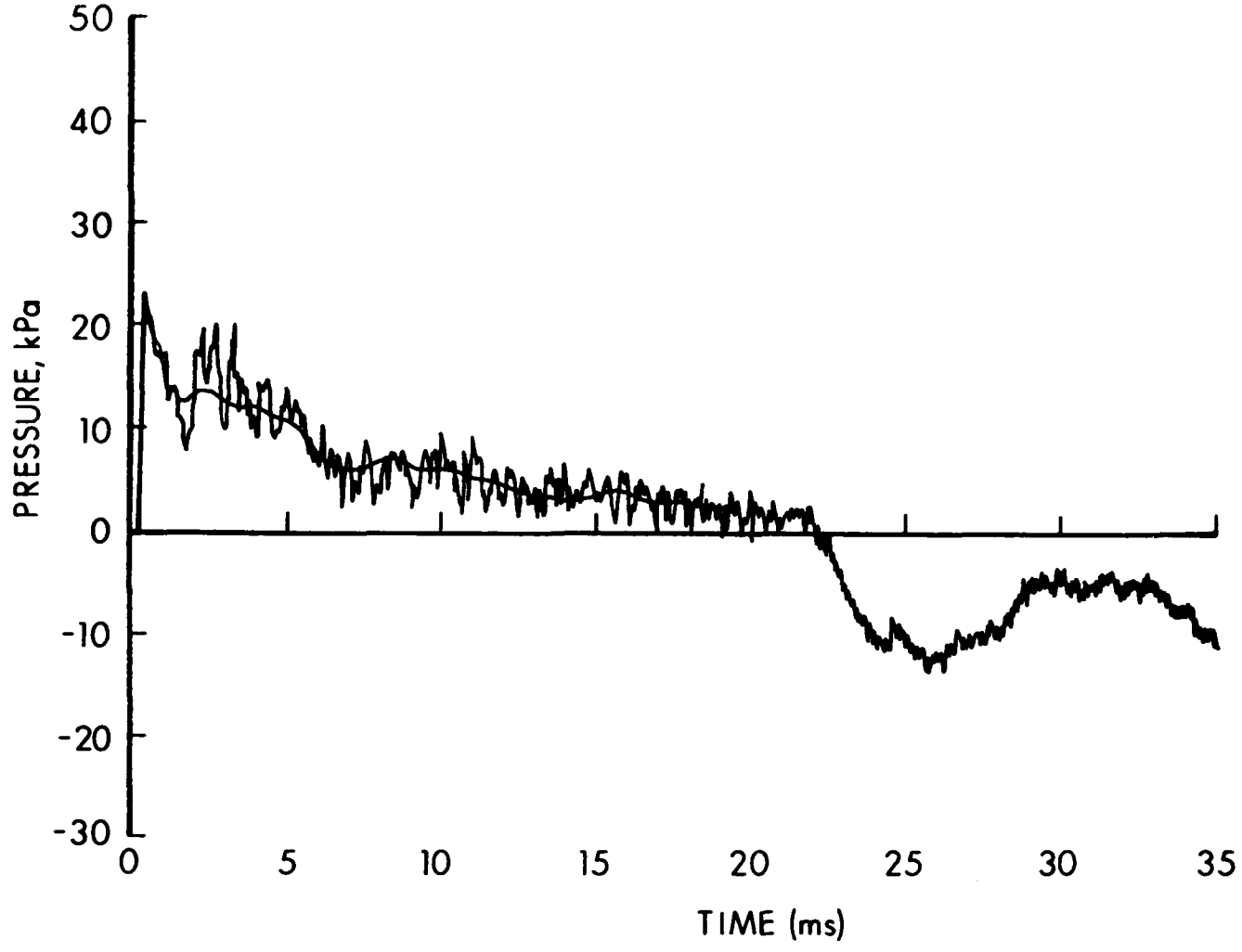

Figure 16. Comparison of Computational/Experimental P-t Histories for Runs

a. P-t Computational/Experimental Comparison, Shot 20

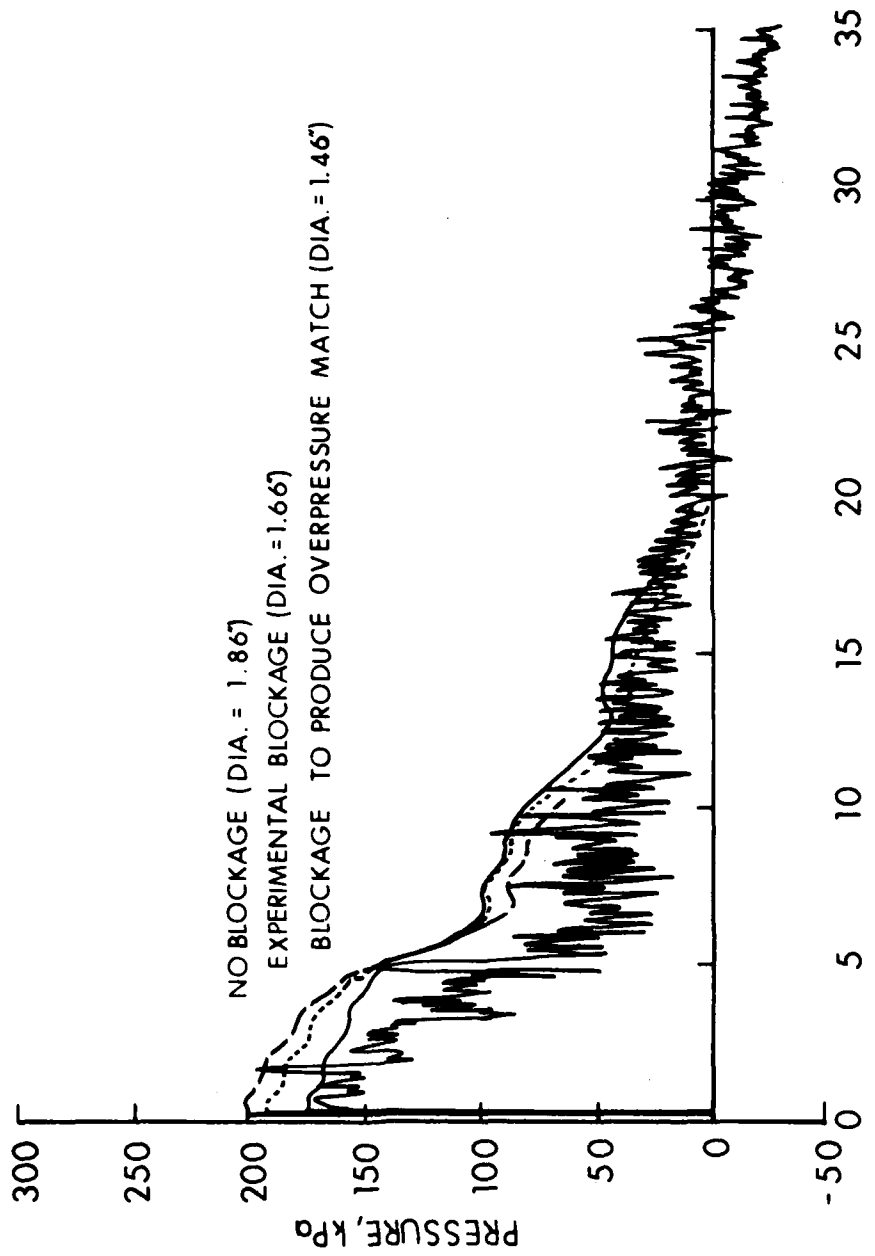

Figure 15. Diaphragm Blockage Effects

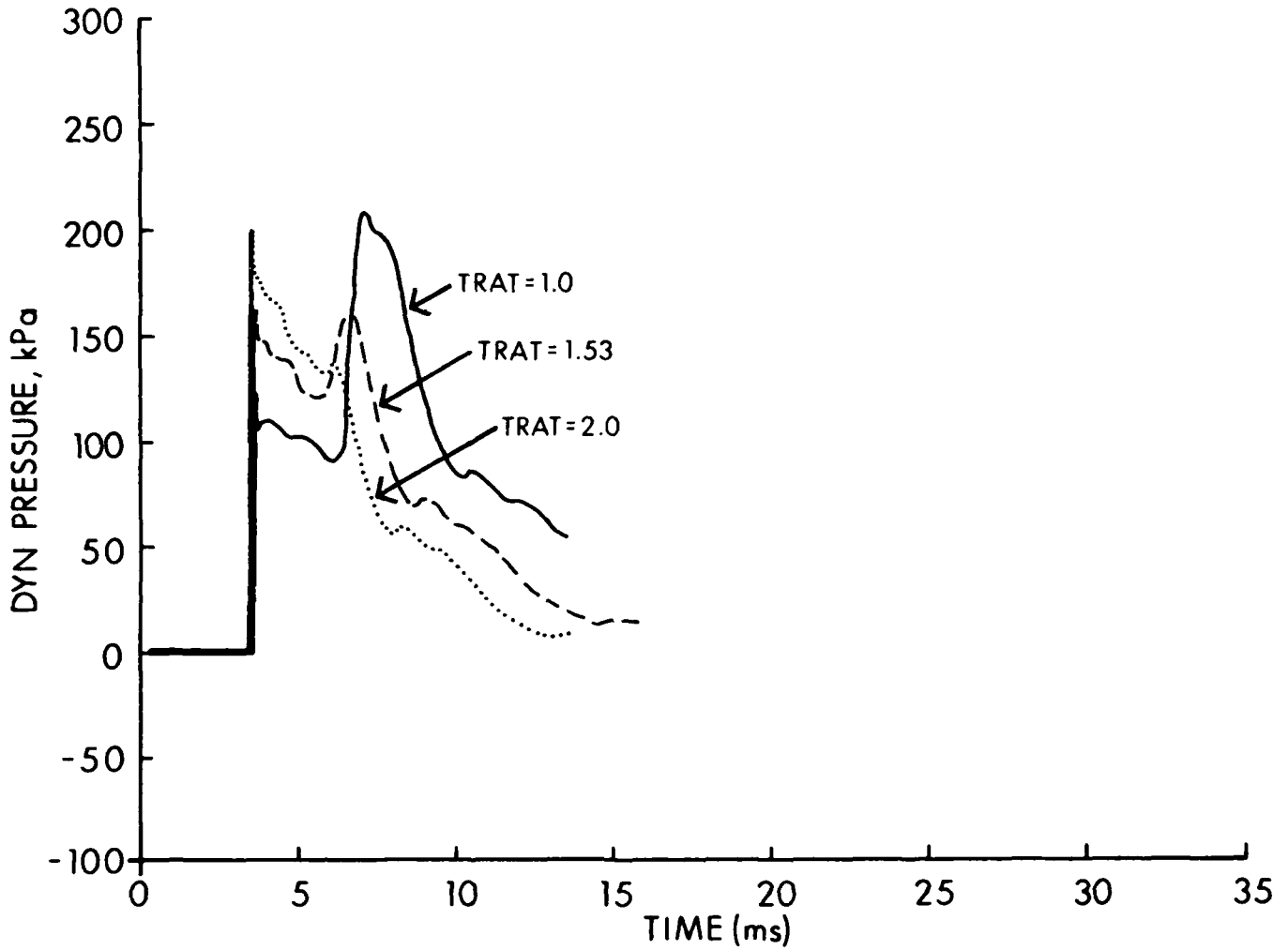

Figure 14. Heated Driver Effects - Dynamic Pressure-Time History

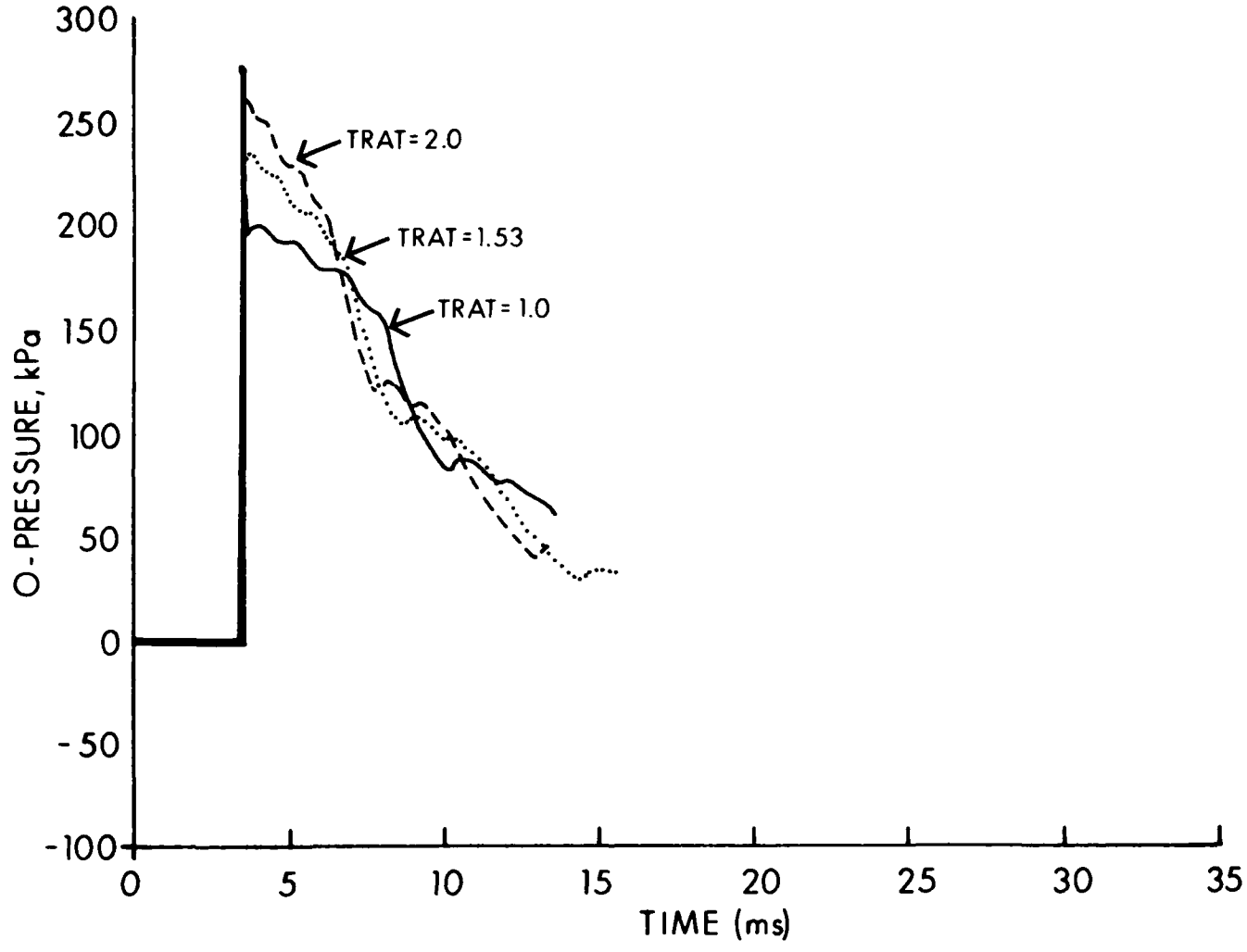

Figure 13. Heated Driver Effects - Pressure-Time History

experimental simulations showed a negligible temperature rise, thus a negligible temperature effect for our operation.

The next effect studied is heating of the driver gas. The driver gas is heated computationally to a temperature ratio of 1.53 and 2.0 for the initial conditions of shot 23. The resultant P-t histories are compared to the original run (temperature ratio of 1.0). As seen in Figure 13, heating of the driver gas causes the shock overpressure to increase and the decay rate to increase. Also, as shown by Figure 14, heating of the driver gas causes the contact discontinuity to decrease.

Finally, diaphragm blockage effects are studied. Experimentally, when the diaphragm breaks, its petals fold back onto the shock tube, thus necking down the throat area. As described in the experimental section, estimates of the open throat area are determined. Computationally, the diaphragm blockage is modeled as a parabolic area contraction. The open throat diameter determined from the measurements is input as the throat diameter of the parabolic area contraction. Figure 15 presents pressure-time histories with various throat diameters for shot 12. The throat diameters modeled are representative of no diaphragm blockage, the diaphragm blockage approximately determined from the measurements, and the diaphragm blockage necessary to produce a shock overpressure match. With no blockage (diameter of nozzle throat = 1.86 inches) the experimental and computational P-t histories are very different. The match becomes better when the blockage effect, as approximately determined from experimental measurement, is modeled (diameter of nozzle throat = 1.66 inches). However, the best match between the experimental and computational P-t histories is for slightly more blockage than was indicated by measurement. An 11.9% reduction (diameter of nozzle throat= 1.46 inches) in the measurement diameter provided a good computational/experimental match. The figure clearly shows that diaphragm blockage effects are important and should be carefully determined and modeled.

D. Comparison of 1-D Computational Predictions to Experimental Results

A comparison of the computationally generated P-t histories and the experimental P-t histories reveals satisfactory agreement.

Shot 20, Figure 16a, represents the lowest pressure shock tube run performed; the driver/driven pressure ratio (PRAT) is 6.9. The computational/experimental match is excellent, even for the spike at the beginning of the waveform, which implies the spike is basically caused by a one-dimensional phenomena.

Shots 2 and 3, Figures 16b and c, represent low pressure shots; driver/driven pressure ratios were 16 and 29 respectively. Agreement after approximately nine milliseconds is excellent. Before nine millisecond, the P-t histories show a spike, that the BRL Q1D Code predicts as smaller in magnitude and duration than is recorded experimentally. Since the code can only predict 1-D phenomena, it seems reasonable that there are 2-D phenomena, possibly Mach reflections, jetting, etc. that occur during the experiment in the diverging nozzle area to enhance the spike formation.

Text continued page 53

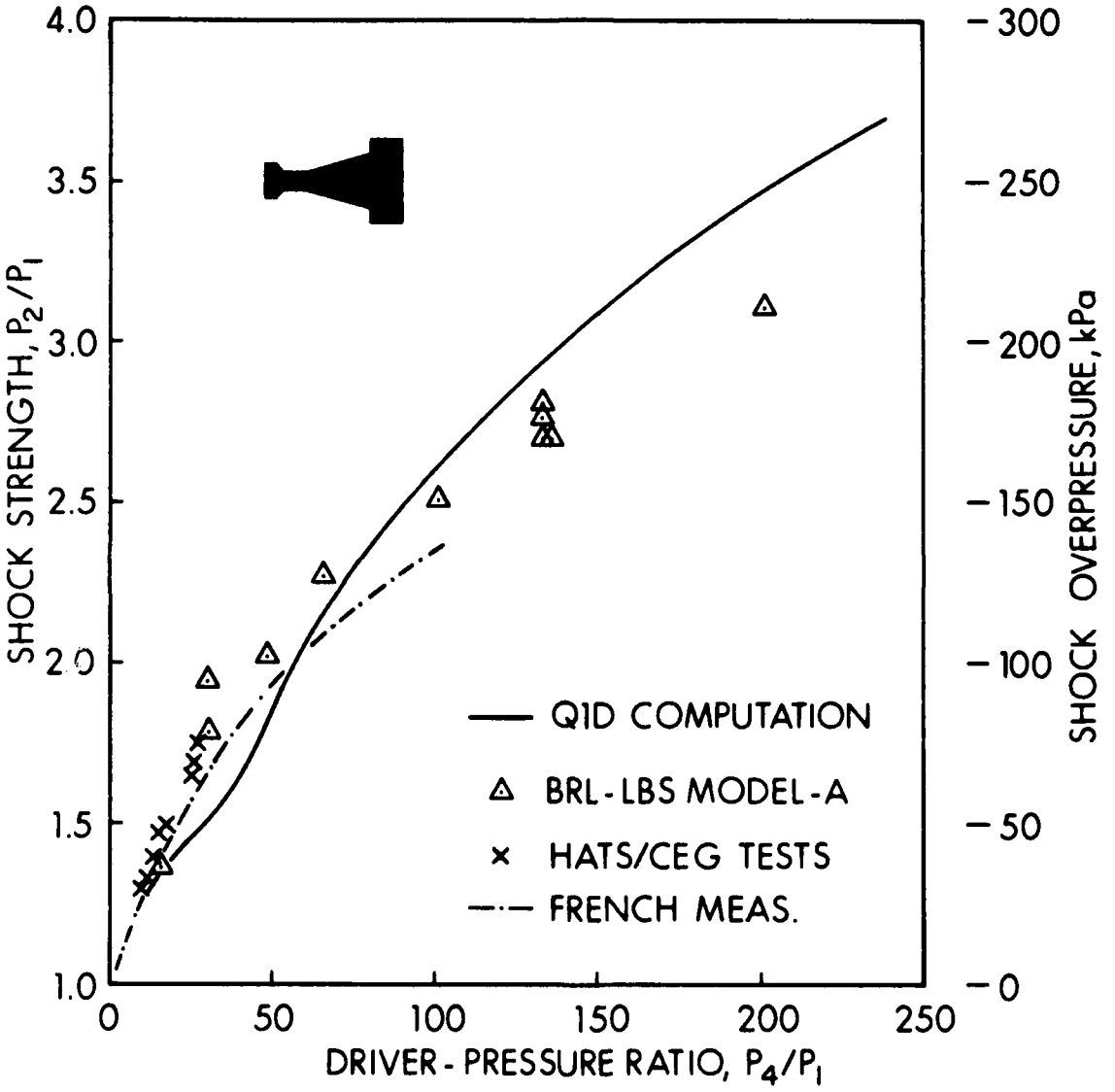

Figure 17. Performance of LBS Model vs. Quasi-1D Prediction

full-scale CEG facility[2,14] are included for perspective. Reasonable to very good correlation is noted between all the data sets at the lower shock levels. At the highest levels the LBS model data is trending below the Q1D calculations. However, as noted in the earlier sections, the calculations consider only an ideal gas flow; possible losses from 2-D and non-ideal effects, eg. viscosity, vortices, etc., plus imperfect tube operation, are not accounted for. Within such limitations, one concludes that the 1D code predicts the LBS model's overall performance quite creditably.

IV. SUMMARY AND CONCLUSIONS

An attempt was made herein to verify predictions of the BRL Q1D Code against the flow from a complicated, non-straight shock tube configuration. With proper accounting for real world behavior, one observes that the computations and experiment agree reasonably well over the full range of shock pressures with respect to pressure levels, pressure histories, appearance of spikes and fluctuations induced by tube geometry, temperature effects on driver due to tube operation procedure, and effects of throat blockage due to diaphragm opening.

Thus the 1-D code provides good performance predictions and correct trends for even very complicated flow geometries, with efficiency and low cost. Further computations utilizing 2-D codes and accounting for 2-dimensional and real gas effects should provide even better agreement but at greater costs in computing time and effort.

ACKNOWLEDGEMENTS

The last two authors (EJG and BPB) wish to thank Messrs R.L. McGill and W.B. Sunderland for their capable and effective assistance with the instrumentation and the acquisition and reduction of data.

[14] *G. Teel, US Army Ballistic Research Laboratory, unpublished data from HATS tests, 1981.*

LIST OF REFERENCES

1. J.R. Crosner and J.B.G. Monzac, "Large Diameter High Performance Blast Simulators." Proc. Fifth Int'l. Symposium on Military Applications of Blast Simulation, Vol. 1, Stockholm, Sweden, May 23-26, 1977.

2. S. Gratias and J.B.G. Monzac, "The Large-Scale Nuclear Blast Simulator of the Gramat Research Center-Concept, Research, Performance." Proc. Seventh Int'l. Symposium on Military Applications of Blast Simulation, Medicine Hat, Canada, July 13-17, 1981.

3. A. Mark, "Computational Design of Large Scale Blast Simulators." AIAA 19th Aerospace Sciences Meeting. St. Louis, Missouri, January 12-15, 1981.

4. H.O. Amann, "Theoretical and Experimental Investigations on the Driving Mechanism of a Shock Wave Simulator of Large Cross Section." Ernest Mach Institute Freiburg, W. Germany, Report No. 2/72 May 1972.

5. H.O. Amann, "Model Tests for a Large Diameter Simulator Driven by Several Generators Filled with Compressed Air." Proc. Fifth Int'l. Symposium on Military Applications of Blast Simulation, Vol. 1, Stockholm, May 23-26, 1977.

6. G. Coulter and others, "Experimental and Computational Modeling of Rarefaction Wave Eliminators Suitable for the BRL 2.44m Shock Tube," US Army Technical Report ARBRL-TR-02503, BRL, APG, MD, June 1983. (AD A131 894)

7. A. Mark, "Computations of Shock Wave Target Interaction," US Army Technical Report ARBRL-TR-02538, BRL, APG, MD, December 1983. (AD B079 280L)

8. R.M. Beam and R.F. Warming, "An Implicit Factored Scheme for the Compressible Navier-Stokes Equations," AIAA J.16, 393-402, April 1978.

9. J. Glimm, "Solution in the Large for Nonlinear Hyperbolic Systems of Equations," Communications in Pure and Applied Mathematics, Vol. 18, 679-715, 1965,

10. T. Saito and I.I. Glass, "Application of Random Choice Method to Problems in Shock and Detonation Wave Dynamics," UTIAS Report No. 240, University of Toronto Institue for Aerospace Studies, Downsview, Ontario, Canada, October 1979.

11. Private Communication from Dr. J.J. Gottlieb, University of Toronto Institute for Aerospace Studies to Dr. A. Mark, Ballistic Research Laboratory, March 1983.

12. J.J. Gottlieb and others, "Use of Perforated Plates in the Driver Section of the BRL 8-ft. Shock Tube to Produce Simulated Blast Waves with Decaying Overpressures," 1st report, 15 March 1983, 2nd report 31 March 1983, 3rd and final report 7 April 1983. University of Toronto Institute for Aerospace studies, Ontario, Canada, M3H 5T6.

13. George A. Coulter, "Shock Pressure Increase in Convergent Ducts," US Army BRL Memorandum Report No. 1625, BRL, APG, MD, January 1965 (AD 463927).

14. G. Teel, US Army Ballistic Research Laboratory, unpublished data from HATS tests, 1981.

DISTRIBUTION LIST

No. of Copies	Organization
12	Administrator Defense Technical Information Center ATTN: DTIC-DDA Cameron Station Alexandria,VA 22304-6145
1	Commander US Army Aviation Research and Development Command ATTN: AMSAV-E 4300 Goodfellow Blvd St. Louis, MD 63120
1	Director US Army Air Mobility Research and Development Command Ames Research Center Moffett Field, CA 94035
2	Director Lewis Directorate US Army Air Mobility Research and Development Lab Lewis Research Center ATTN: Mail Stop 77-5 Cleveland, OH 44135
2	Commander US Army Communications-Electronics Command ATTN: AMDCO-PPA-SA AMSEL-ED Fort Monmouth, NJ 07703
1	Commander US Army Electronics Research and Development Command Technical Support Activity ATTN: DELSD-L Fort Monmouth, NJ 07703-5301
1	Commander US Army Missile Command ATTN: AMSMI-RSS, Mr.Bob Cobb Redstone Arsenal, AL 35898
4	Commander US Army Harry Diamond Labs ATTN: DELHD-TL Mr.J.Meszaros Mr. J. Gwaltney Mr. F.W.Balicki 2800 Powder Mill Road Adelphi, MD 20783
1	Commander US Army Missile Command ATTN: AMSMI-R Redstone Arsenal, AL 35898
1	Commander US Army Missile Command ATTN: AMSMI-YDL Redstone Arsenal, AL 35898
1	Commander US Army Belvoir R&D Center ATTN: STRFB-ND, Mr. R.L. Brooke Fort Belvoir, VA 22060-5606
1	Commander US Army Natick Research and Development Laboratory ATTN: DRDNA-D, Dr.D.Seiling Natick, MA 01760
1	Commander US Army Tank Automotive Command ATTN: AMSTA-TSL Warren, MI 48090
1	Commander Dugway Proving Ground ATTN: STEDP-TO-H,Mr. Miller Dugway, UT 84022
1	Commander US Army Armament, Munitions and Chemical Command ATTN: SMCAR-ESP-L Rock Island, IL 61299

DISTRIBUTION LIST

No. of Copies	Organization
1	DNA Information and Analysis Center Kaman Tempo ATTN: DASIAC 816 State Street P. O. Drawer QQ Santa Barbara, CA 93102
1	Commander Air Force Armament Laboratory ATTN: DLYV, Mr.R.L.McGuire Eglin AFB, FL 32542-5000
1	Ogden ALC/MMRWE ATTN: Mr. Ted E. Comins Hill AFB,UT 84406
1	Commander US Army Tank Automotive Command ATTN: AMSTA-TL Warren, MI 48090
2	HQ, USAF ATTN: IDG/AFISC, (SEW) W.F.Gavitt,Jr. (SEV)Mr.K.R.Shopher Norton AFB, CA 92409
2	Director Joint Strategic Target Planning Staff ATTN: JLTW; TPTP Offutt AFB, NE 68113
1	HQ AFESC/RDC Walter Buckholtz Tyndall AFB, FL 32403
1	AFFDL (FBE) Wright-Patterson AFB, OH 45433
1	Director of Military Applications ATTN: P.O. Matthews Weapons Research Branch DP-225, GTN Department of Energy Washington, DC 20545
1	Commander US Army Foreign Science and Technology Center ATTN: RSCH & Data Branch Federal Office Building 220-7th Street, NE Charlottesville, VA 22901
1	Commander US Army Materials and Mechanics Research Center ATTN: AMXMR-ATL Watertown, MA 02172
1	Director US Army TRADOC Systems Analysis Activity ATTN: ATAA-SL White Sands Missile Range NM 88002
1	Commander US Army Armament R&D Center US Army AMCCOM ATTN: SMCAR-LCM-SP Dover, NJ 07801
1	Commander US Army Materiel Command ATTN: AMCSF 5001 Eisenhower Avenue Alexandria, VA 22333-0001
2	Commander Armament R&D Center US Army AMCCOM ATTN: SMCAR-TSS SMCAR-TDC Dover, NJ 07801
1	Commander Field Command Defense Nuclear Agency ATTN: Tech Lib, FCWS-SC Kirtland AFB,NM 87117

DISTRIBUTION LIST

No. of Copies	Organization
1	Director Benet Weapons Laboratory Armament R&D Ctr, AMCCOM ATTN: SMCAR-LCB-TL Watervliet, NY 12189
1	Commander US Army Research Office P.O.Box 12211 Research Triangle Park NC 27709-2211
1	Director US Army BMD Advanced Tech Ctr ATTN: M.Whitfield P.O.Box 1500 Huntsville, AL 35807
1	Commander US Army Ballistic Missile Defense Sysems Command ATTN: J.Veeneman P.O.Box 1500, West Station Huntsville, AL 35807
1	Commander US Army Engineer Waterways Experiment Station ATTN: WESNP P.O.Box 631 Vicksburg, MS 39180
2	Commander David W. Taylor Naval Ship Research & Development Center ATTN: Mr. A. Wilner, CODE 1747 Mr. W.W.Murray, CODE 17 Bethesda, MD 20084
3	Commander Naval Surface Weapons Center ATTN: Dr.Leon Schindel Dr. Victor Dawson Dr. P.Huang Silver Spring,MD 20910
1	Commander Naval Surface Weapons Center White Oak Laboratory ATTN: R-15, Mr.M.M.Swisdak Silver Spring, MD 20910
1	Commander Naval Surface Weapons Center Dahlgren Laboratory ATTN: E-23, Mr.J.J.Walsh Dahlgren, VA 22448
1	Commander Naval Weapons Center ATTN: Code 0632, Mr. G. Ostermann China Lake, CA 93555
1	Commander Naval Weapons Evaluation Facility ATTN: Document Control Kirtland AFB, NM 87117
1	Commander Naval Research Laboratory ATTN: Code 2027, Tech Lib Washington, DC 20375
2	Superintendent Naval Postgraduate School ATTN: Tech Reports Sec. Code 57, Prof. R.Ball Monterey, CA 93940
1	Commander Bureau of Naval Weapons Department of the Navy Washington, DC 20360
1	Air Force Systems Command/SDOA ATTN: IGFW-840303 Andrews AFB, MD 20334
1	Air Force Armament Laboratory ATTN: AFATL/DLODL Eglin AFB, FL 32542-5000

DISTRIBUTION LIST

No. of Copies	Organization
1	Director Lawrence Livermore Laboratory Technical Information Division P. O.Box 808 Livermore, CA 94550
1	Commander US Army Materiel Command ATTN: AMCDRA-ST 5001 Eisenhower Avenue Alexandria, VA 22333-0001
2	Director Sandia National Laboratory ATTN: Info Dist Div Dr. W.A.von Riesemann Albuquerque,NM 87115
1	Director National Aeronautics and Space Administration Marshall Space Flight Center Huntsville, AL 35812
1	Director National Aeronautics and Space Administration Scientific and Technical Information Facility P. O. Box 8757 Baltimore/Washington International Airport, MD 21240
1	President National Academy of Science ATTN: Mr. D.G. Groves 2101 Constitution Avenue, NW Washington, DC 20418
1	Aeronautical Research Associates of Princeton, Inc. ATTN: Dr. C. Donaldson 50 Washington Road, PO Box 2229 Princeton, NJ 08540
1	Aerospace Corporation P.O.Box 92957 Los Angeles, CA 90009
1	Agbabian Associates ATTN: Dr. D. P. Reddy 250 N. Nash Street El Segundo, CA 90245
2	Battelle Memorial Institute ATTN: Dr. L.E.Hulbert Mr. J.E.Backofen,Jr. 505 King Avenue Columbus, OH 43201
1	Black & Vetach Consulting Engineers ATTN: Mr. H.L.Callahan 1500 Meadow Lake Parkway Kansas City, MO 64114
2	The Boeing Company Aerospace Group ATTN: Dr. Peter Grafton Dr. D. Strome Mail Stop 8C-68 Seattle, WA 98124
1	General American Transportation Corp. General American Research Div. ATTN: Dr. J.C.Shang 7449 N. Natchez Avenue Niles, IL 60648
2	Kaman-AviDyne ATTN: Dr. N.P.Hobbs Mr. S. Criscione Northwest Industrial Park 83 Second Avenue Burlington, MA 01803

DISTRIBUTION LIST

No. of Copies	Organization
1	J.G.Engineering Research Associates 3831 Menlo Drive Baltimore, MD 21215
3	Kaman-Nuclear ATTN: Dr. F.H.Shelton Dr. D.Sachs Dr. R.Keffe 1500 Garden of the Gods Road Colorado Springs, CO 80907
1	Knolls Atomic Power Laboratory ATTN: Dr.R.A.Powell Schenectady, NY 12309
1	Lovelace Research Institute ATTN: Dr.E.R.Fletcher P.O.Box 5890 Albuquerque, NM 87115
2	Martin Marietta Laboratories ATTN: Dr. P.F.Jordan Mr. R.Goldman 1450 S.Rolling Road Baltimore, MD 21227
1	McDonnell Douglas Astronautics Western Division ATTN: Dr. Lea Cohen 5301 Bolsa Avenue Huntington Beach, CA 92647
1	Physics International 2700 Merced Street San Leandro, CA 94577
1	R&D Associates ATTN: Mr. John Lewis P.O.Box 9695 Marina del Rey, CA 90291
1	Science Applications,Inc. 8th Floor 2361 Jefferson Davis Highway Arlington, VA 22202
1	Brown University Division of Engineering ATTN: Prof. R.Clifton Providence, RI 02912
1	Florida Atlantic University Dept. of Ocean Engineering ATTN: Prof. K.K.Stevens Boca Raton, FL 33432
1	Georgia Institute of Tech ATTN: Dr. S. Atluri 225 North Avenue, NW Atlanta, GA 30332
1	IIT Research Institute ATTN: Mrs. H.Napadensky 10 West 35 Street Chicago, IL 60616
3	Southwest Research Institute ATTN: Dr. H.N.Abramson Dr. W.E.Baker Dr. U.S.Lindholm 8500 Culebra Road San Antonio, TX 78228
1	University of Alabama ATTN: Dr. T. L. Cost P. O.Box 2908 University, AL 35486
1	University of Delaware Department of Mechanical and Aerospace Engineering ATTN: Prof J.R.Vison Newark, DE 19711

DISTRIBUTION LIST

No. of Copies	Organization
1	HQDA DAMA-ART-M Washington, DC 20310
1	Commandant US Army Infantry School ATTN: ATSH-CD-CSO-OR Fort Benning, GA 31905
1	Commander US Army Development & Employment Agency ATTN: MODE-TED-SAB Fort Lewis, WA 98433
1	AFWL/SUL Kirtland AFB, NM 87117

Aberdeen Proving Ground

Dir, USAMSAA
ATTN: AMXSY-D
AMXSY-T, Mr.R.Norman
AMXSY-MP, H.Cohen
Cdr, USATECOM
ATTN: AMSTE-TO-F
Cdr, US Army Toxic and Hazardous Materials Agency
ATTN: AMXTH-TE

Cdr, CRDC, AMCCOM
ATTN: SMCCR-RSP-A
SMCCR-MU
SMCCR-SPS-IL

USER EVALUATION SHEET/CHANGE OF ADDRESS

This Laboratory undertakes a continuing effort to improve the quality of the reports it publishes. Your comments/answers to the items/questions below will aid us in our efforts.

1. BRL Report Number_____ Date of Report_____

2. Date Report Received_____

3. Does this report satisfy a need? (Comment on purpose, related project, or other area of interest for which the report will be used.)_____

_____

_____

4. How specifically, is the report being used? (Information source, design data, procedure, source of ideas, etc.)_____

_____

_____

5. Has the information in this report led to any quantitative savings as far as man-hours or dollars saved, operating costs avoided or efficiencies achieved, etc? If so, please elaborate._____

_____

_____

6. *General Comments. What do you think should be changed to improve future* reports? (Indicate changes to organization, technical content, format, etc.)

_____

_____

_____

CURRENT ADDRESS

_____
Name

_____
Organization

_____
Address

_____
City, State, Zip

7. If indicating a Change of Address or Address Correction, please provide the New or Correct Address in Block 6 above and the Old or Incorrect address below.

OLD ADDRESS

_____
Name

_____
Organization

_____
Address

_____
City, State, Zip

(Remove this sheet along the perforation, fold as indicated, staple or tape closed, and mail.)

— — — — — — — — FOLD HERE — — — — — — — — — —

r
Ballistic Research Laboratory
AMXBR-OD-ST
n Proving Ground, MD 21005-5066

NO POSTAGE
NECESSARY
IF MAILED
IN THE
UNITED STATES

ICIAL BUSINESS
FOR PRIVATE USE, $300

BUSINESS REPLY MAIL
FIRST CLASS PERMIT NO 12062 WASHINGTON, DC

POSTAGE WILL BE PAID BY DEPARTMENT OF THE ARMY

Director
US Army Ballistic Research Laboratory
ATTN: AMXBR-OD-ST
Aberdeen Proving Ground, MD 21005-9989

— — — — — — — — FOLD HERE — — — — — — — — — —

END

FILMED

10-85

DTIC